THE JASMINE PILOT STUDY

BY P. J. WEBSTER, E. F. BRADLEY, C. W. FAIRALL, J. S. GODFREY, P. HACKER, R. A. HOUZE JR., R. LUKAS, Y. SERRA, J. M. HUMMON, T. D. M. LAWRENCE, C. A. RUSSELL, M. N. RYAN, K. SAHAMI, AND P. ZUIDEMA

A recent field experiment aimed at supplying critical data from the Indian Ocean region may eventually help climate models reproduce and forecast the intraseasonal and interannual variability of the monsoon

At a workshop on the variability of the Asian–Australasian Monsoon in July 1998 in St. Michaels, Maryland, two major mechanisms were discussed at length, each thought to have the potential to produce monsoon variability.[1] The first mechanism, the role of external forcing (e.g., Charney and Shukla 1980), considered the influence on the monsoon of ENSO variability, local sea surface temperature anomalies, and ground moisture content. The second mechanism involved the role higher-frequency (intraseasonal) hydrodynamical instabilities of the monsoon circulation might play in producing interannual variability of the system. Figure 1a shows time–latitude plots of the Microwave Sounding Unit (MSU) satellite precipitation product along 90°E for the spring and summer of 1988. Monsoon precipitation often appears first at the equator before propagating northward as originally discovered by Sikka and Gadgil (1980). Within the context of the second question discussed at the workshop, it was asked whether these intraseasonal oscillations were controlled and modified by large-scale planetary forcing or were the intraseasonal instabilities themselves determining interannual monsoon variability? The latter question arises from the numerical studies of Ferranti et al. (1997) and the observational analyses of Hendon et al. (1999) for the Australian monsoon and Lawrence and Webster (2001) for the south Asian monsoon.

These questions largely define the limiting factor for predicting monsoon variability. The monsoon may be a slave to other climate components, like ENSO, or may have its own modes of variability resulting, perhaps, from the coupling of land, atmospheric, and oceanic variability. It may be a hybrid that is forced remotely to some extent yet contains its own local modes of variability, which may include chaotic

[1] Proceedings of the workshop on "The Variability of the Asian-Australian Monsoon" can be viewed online at http://paos.colorado.edu/~webster.

AFFILIATIONS: WEBSTER, LAWRENCE, SAHAMI, AND ZUIDEMA—Program in Atmospheric and Oceanic Sciences, University of Colorado, Boulder, Colorado; BRADLEY—Division of Land and Water, Commonwealth Scientific and Industrial Research Organisation, Canberra, Australia; FAIRALL, RUSSELL, AND RYAN—NOAA Environmental Technology Laboratory, Boulder, Colorado; GODFREY—Division of Marine Science, Commonwealth Scientific and Industrial Research Organisation, Hobart, Australia; HACKER, LUKAS, AND HUMMON—School of Ocean and Earth Sciences and Technology, University of Hawaii at Manoa, Honolulu, Hawaii; HOUZE AND SERRA—Department of Atmospheric Sciences, University of Washington, Seattle, Washington.
CORRESPONDING AUTHOR: P. J. Webster, School of Earth and Atmospheric Sciences, Georgia Institute of Technology, 221 Bobby Dodd Way, Atlanta, GA 30332-0340
E-mail: pjw@eas.gatech.edu
DOI: 10.1175/BAMS-83-11-1603

In final form 6 August 2002

(a) MSU precipitation (mm/day) along 90°E for spring-summer of1988

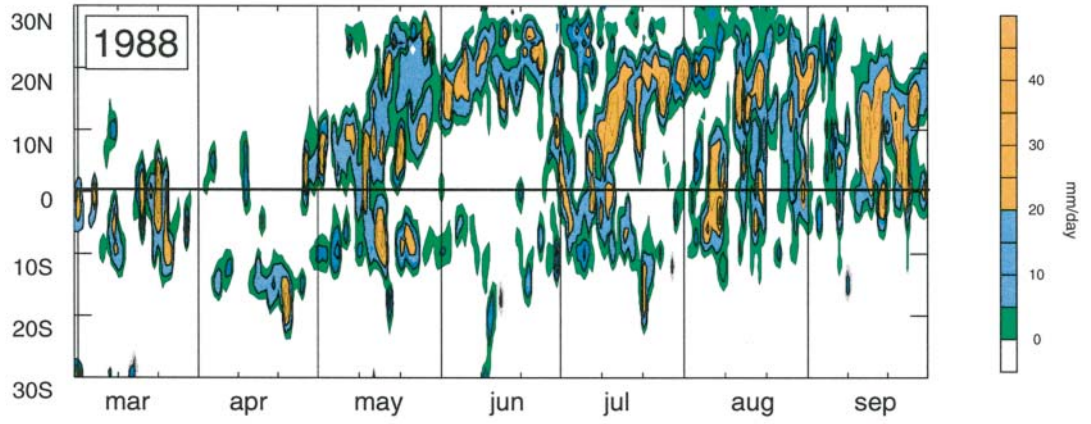

(b) Modelled mean meridional ocean heat transport across Indian Ocean for spring and summer of 1988 (PW)

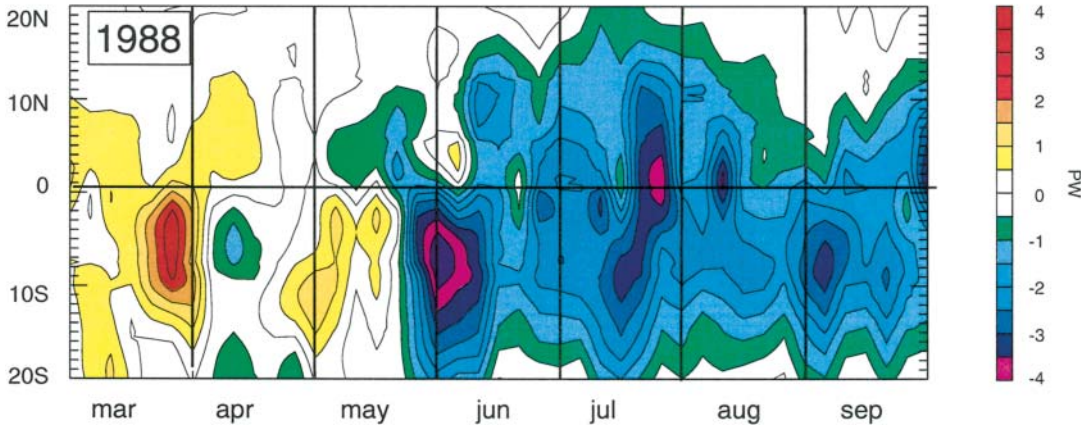

(c) Composite MSU precipitation along 89°E with proposed cruise path

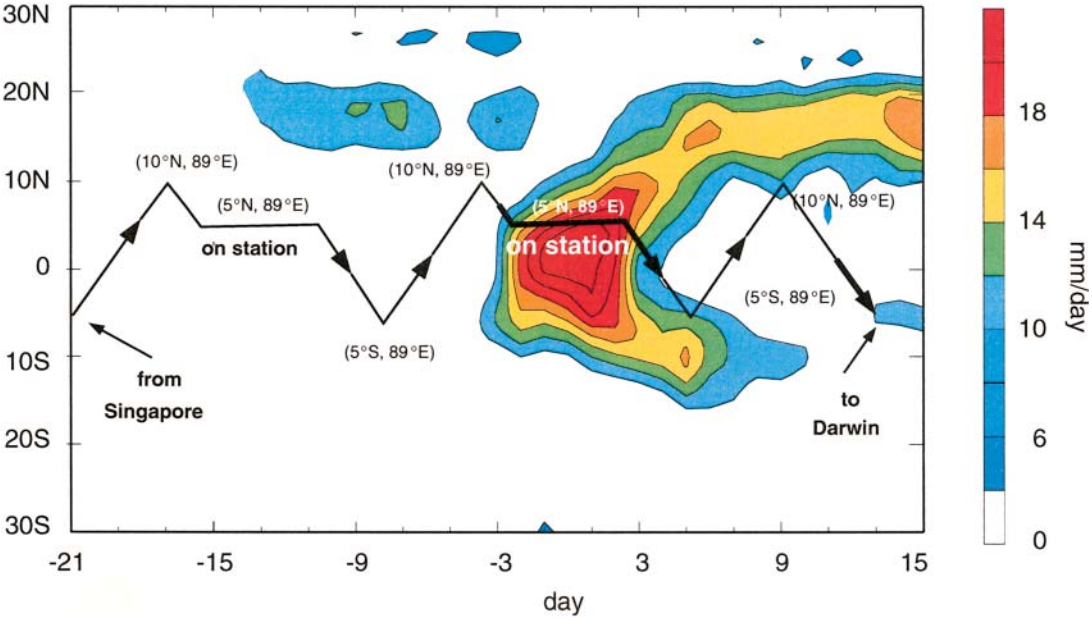

elements, that are modified by the remote forcing (Palmer 1994; Webster et al. 1998).

Advances are limited by the lack of data in the region and an inability to identify the fundamental processes that create the variability. Little is known about the state of the upper Indian Ocean other than its surface temperature and its surface height. Despite a few field campaigns [from the Indian Ocean Experiment (INDOEX) in the late 1970s during the First GARP (Global Atmospheric Research Program) Global Experiment (FGGE) to the World Ocean Circulation Experiment (WOCE) Indian Ocean Experiment] and some repeat expendable bathythermograph (XBT) lines, there have been relatively few direct measurements in the Indian Ocean Basin. Despite climatologies of ship observations (e.g., Oberhuber 1988), research quality observations, such as those reported by Wyrtki (1971) and Hacker et al. (1998) for the eastern Indian Ocean during winter, are rare.

It is clear that more data is needed to establish relationships between the atmosphere and ocean on intraseasonal timescales, which have proven important in other oceans (Lukas and Lindstrom 1991; Vialard and Delecluse 1998; Masson et al. 2002). For instance, research in the Pacific warm pool had shown the importance of the salt-stratified barrier layer in complex atmosphere–ocean interactions.[2] This shallow salinity stratification concentrates heat and momentum in the upper layer of the western Pacific (Lukas and Lindstrom 1991). Vialard and Delecluse (1998) showed that westerly wind bursts propel the barrier layer eastward, moving the impacts of the insulating layer to other regions of the warm pool every month or so. This movement might favor the growth of unstable air–sea interactions in the central Pacific. Thus Vialard and Delecluse (1998) and Masson et al. (2002) argue that the transience of the barrier layer is a key to coupled ocean–atmosphere instabilities and we expect it to be equally significant to intraseasonal oscillations in the summer monsoon.

There are additional reasons for conducting research in the eastern Indian Ocean. The region has great oceanographic significance. It is the exit region of the Indonesian throughflow that connects the Pacific and the Indian Oceans. Here, the very saline waters of the western Indian Ocean and the freshwater of the eastern basin mix, determining salt balance for the entire basin. The eastern Indian Ocean is also a region of considerable dynamic activity. Upper-ocean currents reverse on seasonal and intraseasonal timescales, and the region also contains a pole of the newly discovered Indian Ocean zonal mode, or Indian Ocean "dipole" (Webster et al. 1999; Saji et al. 1999; Yu and Rienecker 1999, 2000; Webster et al. 2001). Furthermore, there appears to be a substantial oceanic barrier layer even stronger than that originally documented in the Pacific Ocean by Lukas and Lindstrom (1991). Hacker et al. (1998) observed a barrier layer in the Bay of Bengal in the northeast (winter) monsoon, which would be expected to persist through summer as precipitation (freshening) increases.

The eastern Indian Ocean is also critical from an atmospheric perspective, with precipitation extremes

[2] Traditionally, it was assumed that in the upper ocean the depth over which temperature is uniform determines the depth of the ocean mixed layer. However, in the Tropics there is often a change in density in the isothermal layer that is the result of a fresh surface layer overlying a more saline layer. The layer between the halocline and the thermocline is referred to as the barrier layer (Lukas and Lindstrom 1991) because of its impact on the heat budget of the upper ocean.

FIG. 1. (a) Intraseasonal variability of the monsoon as depicted by daily MSU precipitation along 90°E plotted against latitude as a function of time for the boreal late spring and summer of 1988. Beginning in early summer, precipitating events begin near the equator and extend poleward in each hemisphere. The northward extension of the equatorial precipitation becomes the active period of the monsoon while the southward extension produces precipitation in the Southern Hemisphere. Thirty-nine such events were identified in the 1984–95 period (Webster and Tomas 1999). (b) Zonally integrated heat flux averaged across the Indian Ocean, after Loschnigg and Webster (2000). The model used is an intermediate ocean model of McCreary et al. (1993) forced by 5-day-average winds and insolation from the NCEP–NCAR reanalyses. (c) Composite precipitation pattern associated with monsoon intraseasonal oscillations as a function of time and latitude, based on 39 monsoon intraseasonal events identified by Webster and Tomas (1999). The pattern was used for experiment design with the proposed cruise path shown as a black line. Plans called for sampling the atmosphere and ocean in an "undisturbed" state before the advent of an monsoon intraseasonal oscillation, and in the "disturbed" state after the monsoon intraseasonal oscillation had formed. Two sampling techniques were planned: north–south transects along 89°E and two "on-station" periods near 5°N. As it turned out, the sequence of meteorological events encountered in the eastern Indian Ocean followed the composite almost exactly (see Fig. 4b). The only change to the plan was to locate the on-station period farther to the north in fresher water.

falling in the northern Bay of Bengal and just south of the equator (Fig. 1a). In fact, satellite estimates indicate that the northern Bay of Bengal receives the largest mean precipitation in south Asia during the summer monsoon. Intraseasonal oscillations of the monsoon also reach maximum amplitude in the eastern Indian Ocean (Lawrence and Webster 2002). It is a source for "active" periods of the monsoon (with enhanced precipitation) and "break" periods (with short-lived droughts or lulls in the precipitation rate). Furthermore, the biennial oscillation possesses strong signals in the eastern Indian Ocean (Meehl 1994) and is a center of strong interannual rainfall variance. While many of these features have been known to exist for a very long time (see reviews by Godfrey 1995; Webster et al. 1998), the physical processes that maintain them are not understood.

Recent ocean modeling studies forced by the National Centers for Environmental Prediction and National Center for Atmospheric Research (NCEP–NCAR) reanalysis winds suggest that there is a substantial basinwide response by the ocean to intraseasonal wind forcing. Figure 1b (from Loschnigg and Webster 2000) shows the zonally averaged meridional heat transport as a function of latitude for the summer and spring of 1988. Oscillations of 2–3 PW (petawatt: 10^{15} W) occur over the space of weeks and on similar timescales to the precipitation variations (and the associated wind variations) shown in Fig. 1b. Yet, we do not have the data to see if these very large intraseasonal heat transports are an artifact of the model or whether they represent integral parts of the Indian Ocean heat balance.

The potential rewards for increasing our understanding of the monsoon climate are substantial. Forecasting variability of monsoon rainfall from year to year with sufficient lead time would allow remedial action by managers of agricultural and water resources. But forecasting the onset of the monsoon and the occurrence, magnitude, and duration of active and break periods during a monsoon season 10–14 days in advance may have a far greater potential impact on an agrarian society than forecasting whether or not the entire monsoon summer rainfall may be anomalous (A. B. Subbiah, Asian Disaster Preparedness Center, Bangkok, Thailand, 2001, personal communication). Plowing and planting periods are extremely vulnerable. Once the monsoon begins, the timing of the first break becomes critical. Even if the average seasonal monsoon rains are normal, an ill-timed break in the rain can devastate a local economy (Webster et al. 1998).

It has been argued that interannual variability of large-scale climate systems such as the monsoon and ENSO cannot be understood without comprehending the physical processes that control the annual cycle (e.g., Webster and Yang 1992). By extension, it can also be argued that the annual cycle of the monsoon cannot be understood (or perhaps predicted) without a thorough knowledge of the physics of intraseasonal variability. Indeed, intraseasonal variability appears to be a fundamental building block of both the annual cycle and its interannual variability (Ferranti et al. 1997).

Following this chain of logic, it is probably not a coincidence that the inability of numerical models to simulate the mean seasonal precipitation patterns of the regional monsoons (Sperber and Palmer 1996; Gadgil and Sanjani 1998) is matched by the model's inability to possess realistic intraseasonal variability, or any variance at all at these timescales (Slingo et al. 1996). In summary, understanding the physical processes that produce intraseasonal variability in the monsoon stands as the fundamental problem in monsoon climate studies.

The Joint Air–Sea Monsoon Interaction Experiment (JASMINE) held in the eastern Indian Ocean during the summer of 1999 partially addressed these data needs with a variety of observational equipment and strategies. In particular JASMINE addressed this issue of the intraseasonal variability of the monsoon. JASMINE was a new and significant step in identifying and measuring these fundamental coupled processes in the monsoon system. JASMINE was designed to provide basic information about the oceanic and atmospheric character of the monsoon intraseasonal oscillation. JASMINE measured the heat, moisture, and momentum fluxes between the atmosphere and the ocean, the evolving state of the upper ocean, and the organization of convection and its interaction with the larger-scale environment. The project aimed to document these fluxes throughout the transitions between active and break periods of the monsoon, as well as to document during these periods the upper-ocean velocity, temperature and salinity structures, and the upper-ocean budgets of heat and salt. JASMINE was also designed to acquire statistics of surface turbulent and radiative fluxes for comparison with previous tropical Pacific field programs. Furthermore the program aimed to document and acquire statistics of convection in order to understand the nature and organization of cloud systems during active and break periods of the monsoon and to compare these statistics with convective organizations in other dynamic regimes in the Tropics.

JASMINE followed INDOEX (Ramanathan et al. 2001) where aerosols originating over south Asia were

documented. Also, in July 1999 Indian scientists conducted a national joint meteorology–oceanography experiment [the Bay of Bengal Monsoon Experiment (BOBMEX) Bhat et al. 2001] in roughly the same location as JASMINE. During 1999, the European geostationary satellite *METEOSAT-5* was relocated over the central Indian Ocean to provide an unprecedented view of the monsoon. The summer of 1999 was a unique season for observation of the coupled ocean–atmosphere system in the eastern Indian Ocean.

IMPLEMENTATION OF JASMINE. The field phase of JASMINE was held in the eastern Indian Ocean and the southern Bay of Bengal for a total of 52 days during April, May, June, and September 1999 (excluding transit times), having acquired an additional two weeks of ship time following INDOEX while the National Oceanic and Atmospheric Administration (NOAA) ship *Ronald H. Brown* (hereafter referred to as the *Brown*) relocated from the Maldives to Singapore (see Table 2). In the April–June period, the *Brown* was used. During September, the Australian research vessel *Franklin* (the *Franklin*) operated in the region. JASMINE was planned for the eastern Indian Ocean and southern Bay of Bengal for 12 May–20 June aboard the *Brown* and in September aboard the *Franklin*. These periods were chosen to maximize the chances of encountering a full cycle of an intraseasonal oscillation as documented by Webster and Tomas (1999).

The project featured an ensemble of in situ and remote sensing instruments to measure the ocean and atmosphere. A summary of instrumentation on the *Brown* is given in Table 1 with many of the instruments identified in Fig 2. Collectively, measurements were made with Global Positioning System (GPS) rawinsondes, bulk near-surface meteorological measurements, fast-response meteorological instruments, radiometers, numerous rain gauges, three profiling Doppler radars, microwave and IR radiometers, a cloud ceilometer, and a scanning C-band Doppler precipitation radar. The state of the upper ocean was measured using conductivity–temperature–depth (CTD) instruments, near-surface thermosalinographs, and current profilers (see the sidebar).

In addition to the data collected from the ships, high-resolution satellite data from *NOAA-12, NOAA-14,* and *NOAA-15* was accessed aboard the *Brown*. Furthermore, the European geostationary satellite *METEOSAT-5* was repositioned over the Indian Ocean for INDOEX and remained operational throughout JASMINE. The 3-hourly data for the JASMINE period was made available to JASMINE investigators by the European Space Agency after the experiment. Also, the European Centre for Medium-Range Weather Forecasts (ECMWF) provided 3-hourly analyses at standard levels and single-point data to the investigators.

The aim of the operations plan was to sample changes in the ocean–atmosphere system through the full life cycle of a monsoon intraseasonal oscillation. Because of the lack of modern, high-quality upper-ocean observations in the Bay of Bengal sector of the Indian Ocean during the onset of the southwest monsoon, the ocean-specific goals were to document the time-varying meridional structure of the temperature, salinity, and velocity fields including the mixed-layer and barrier-layer structures from 5°S to 10°N, and to estimate upper-ocean heat and freshwater budgets within the Bay of Bengal during the active and break periods. Figure 1c shows the course originally planned for the research vessel, namely, a latitude–time section along 89°E relative to the composite monsoon intraseasonal oscillation determined from the 39 intraseasonal oscillations of the monsoon identified by Webster and Tomas (1999). Using satellite information received aboard the ship, it was planned to adjust the scheme in the field to match actual conditions. In fact this proved unnecessary as the weather encountered matched the composite remarkably well.

The experimental design called for a series of north–south transects near 89°E that ensured that the *Brown* and *Franklin* remained in international waters between 5°S and 10°N. The additional two weeks of shiptime (previously mentioned) aboard the *Brown* in April 1999 allowed the measurement of oceanic conditions during the early phase of the monsoon onset. This first transect captured a strong westerly wind burst in the equatorial region. Data from this period is called phase I. After the port stop in Singapore, the phase II observations were conducted during May 1999. Two small-scale surveys (star 1 and star 2) near 10°N, 89°E were made during phase II of JASMINE for periods of 5 days each. The star patterns were designed to estimate terms in the upper-ocean heat and salt budgets (see Fig. 3 and Tables 2, 3). The *Franklin* observations in September 1999 (phase III) included a similar survey in a similar location, but using triangular patterns following a floating buoy drogued in the upper ocean.

INITIAL RESULTS FROM THE FIELD PHASE. *Synoptic situation.* During phase I in April (Fig. 4a), a relatively weak disturbance persisted in the Bay of Bengal with the ship passing through the dis-

Table 1. Observation system on the *Brown*. Left-hand column indicates the instrument number that is used to show the location of the instrument in Fig. 1. The second column lists the instruments and the third column shows its utility. Basic references for the instrumentation are given in the last column.

	SYSTEM	MEASUREMENT	REFERENCES
1	Air–sea flux system	Motion corrected turbulent fluxes	Fairall et al. (1996, 1997); Edson et al. (1998)
2	Pyranometer and pyrgeometer	Downward solar radiative, IR flux	Godfrey et al. (1999); Fairfall et al. (1998)
3	Bulk meteorology	SST, air *T,* RH, wind speed, and direction	Fairall et al. (1996, 1997); Godfrey et al. (1999)
4	Ceilometer	Cloud-base height	Fairall et al. (1997)
5	0.92- and 3-GHz Doppler	Wind and precipitation profiles radar profiler	Eklund et al. (1988, 1997); Gage et al. (1996, 1999)
6	Rain gauges	Rain rate	Fairall et al. (1996)
7	Rawinsonde	Wind, temperature, humidity profiles	NCAR ATD
8	35-GHz Doppler cloud radar	Cloud microphysical properties	Moran et al. (1998); Frisch et al. (1995)
9	20- and 31-GHz wave radiometer	Integrated cloud liquid water, total vapor	Snider and Hazen (1998); Hogg et al. (1983)
10	WHOI LICOR 6262 system	Fast CO_2 air concentrations	Fairall et al. (2000)
11	Upward-pointed IR thermometer	Cloud-base radiative temperature	
12	BNL portable radiation	Direct and diffuse solar, IR fluxes	
13	Scanning C-band Doppler radar	Precipitation 3D structure, wind	KWAJEX (1999)
14	CTD	Ocean *T, S* profiles	Lukas et al. (2001): Godfrey et al. (1999)
15	ADCP	Ocean current profiles	
16	Satellite/SCS	NOAA, GMS data	
17	Navigation/SCS	Position, course, speed, heading, etc.	
18	Thermosalinograph	Near-surface *T, S*	
19	AOML underway CO2 system	Water–air CO_2 concentrations	Fairall et al. (2000)
20	Autosal	Water salinity calibrations	
21	Floating thermistor	Near-surface (5 cm) sea temperature	Fairall et al. (1996); Donlon et al. (1998)

turbance near UTC (Julian) day 103. The first half of phase II (Fig. 4b) encountered only minimal convection and was, consequently, a period of high insolation. However, during the second half of phase II the atmosphere was greatly disturbed with extensive deep convection. During this time a monsoon intraseasonal oscillation, in a manner similar to that seen in Fig. 1a, propagated northward. The monsoon intraseasonal oscillation encountered during the JASMINE field phase (Fig. 4b) was similar to the composite oscillation in Fig. 2. The brightness temperature distributions show that the range of weather during phase II fulfilled the requirements set out in the planning. Phase III (Fig. 4e) was essentially a quiescent period during the late summer monsoon.

The preonset and the active monsoon periods encountered in JASMINE appear similar to active and break periods in the established monsoon (e.g., Webster et al. 1998). For example. the buoy data from the Indian surface moorings in the Bay of Bengal (Sengupta and Ravichandran 2001; Bhat et al. 2001; Sengupta et al. 2001) show SST oscillations on intraseasonal timescales of about 1.5°C that match those observed during JASMINE. Also, using surface wind data from NCEP–NCAR reanalysis and outgoing longwave radiation (OLR) data indicates that the conditions in each phase were representative of active and break periods (Table 5). Compared to a climatology of active and break periods, the star 2 period was indicative of a stronger than average active period. Star 1

Structure of the upper ocean was measured by a variety of instruments. Two sea-bird CTD instruments (14) were used to measure upper-ocean structure: the *Brown's* shipboard single sensor system during the April 1999 leg, and the University of Hawaii's dual temperature/conductivity sensor system during the May–June 1999 leg. All sensors were calibrated before and after the cruise, and have measurement accuracies better than 0.01°C (temperature) and 0.01 psu (salinity) below 5 m. The *Brown's* thermosalinograph (18) provided continuous, high-resolution measurements of temperature and salinity in the surface layer at a depth of 5.6 m. Horizontal currents over the depth range of 17–400 m, typically, were measured with the ship's RDI 150-kHz narrowband acoustic Doppler current profiler (ADCP) together with a Ring LASER gyroscope and P-code navigation. The ADCP data were stored as 2-min ensembles with a vertical resolution of 8 m. A total of 25 surface drifters were deployed as part of the global drifter array to measure near-surface currents and temperatures, and two solo-type profiling temperature and salinity floats were deployed from the *Brown* during JASMINE. Upper-ocean data collected during JASMINE is documented by Lukas et al. (2001) and available online at http://www.soest.hawaii.edu/JASMINE/.

One of the unique characteristics of the *Brown* is the permanently installed, stabilized scanning C-band Doppler radar. The C-band reflectivity observations document the basic three-dimensional structure of the precipitation patterns. Single Doppler measures radial velocity and the observations can be used to determine the circulation of convective and mesoscale systems. Analysis of this basic documentation, enables the determination of the key levels in the atmosphere where convective systems interact with the large-scale circulation (Kingsmill and Houze 1999a,b). The range of the radar is about 240 km, although the effective range for Doppler determinations is approximately 100 km. The C-band has a 5-cm wavelength and a 1° beamwidth. Both surveillance and volume scans were used during JASMINE and were designed to provide comparisons with the upward-looking cloud radar described below. Details of the volume scan sets are available online at http://www.atmos.washington.edu/~serra/JASMINE/jasmine_overview.html.

Profiling Doppler radars and radiometers on the *Brown* helped define the structure of the marine boundary layer and to provide diagnostics of precipitating systems. The *Brown* carried a 915-MHz wind profiler, a 3-GHz S-band precipitation profiler, and a 35-GHz (K band) profiling Doppler cloud radar with a short wavelength (8 mm) making the radar sufficiently sensitive to observe cloud droplets (thus, it is often referred to as a "cloud radar"). JASMINE is only the second deployment of a cloud radar on a ship. It was used in combination with a microwave radiometer for retrieving total integrated vapor and integrated water. The radiometer is an essential complement to the cloud radar for retrievals of cloud droplet size information (Frisch et al. 1995). Additional cloud information was obtained from a commercial lidar ceilometer, which is not "blinded" by precipitation so it is more capable of detecting cloud base than the cloud radar.

While single-Doppler radar observations are useful in analyzing the interaction of convective and large-scale circulations, observations of the ambient large-scale thermodynamic and wind stratification in the vicinity of the mesoscale convective systems are also necessary. To meet these needs, a series of upper-air soundings were taken from the *Brown*. The GPS tracking system provided great accuracy in wind measurements. In conjunction with the soundings, high-frequency surface meteorology measurements were maintained aboard the ship. A similar system was used on the *Franklin*. Overall, 272 successful radiosonde ascents were undertaken (Table 3). Over 95% of the soundings reached the Global Telecommunications System and were used as initial data by major numerical centers throughout the world.

The *Franklin* carried an identical flux system to that on the *Brown*. The location of instruments on the *Franklin* was generally as illustrated in Godfrey et al. (1999, see their Fig. 5), although no SeaSoar or buoy was deployed in JASMINE. The ship was equipped with a boom that extended 10 m forward of the bow to carry instruments clear of ship's influence. Other instruments were mounted on an arm near the top of the foremast and some were located at various positions along the yardarm on the main mast. The *Franklin* oceanographic measurement system mirrored that of the *Brown*, except that (i) the CTD used was a Neil Brown Mark III and (ii) the *Franklin* measurements included nitrate and phosphate samples and bottle samples of salinity.

represented a strong break period. In this context, a "strong break period" is one with higher-than-average OLR and lower-than-average surface wind speed.

Moderate winds during the first northward transect in phase II lessened to < 6 m s^{-1} during star 1 (Fig. 5). Moderate upper-tropospheric easterlies were

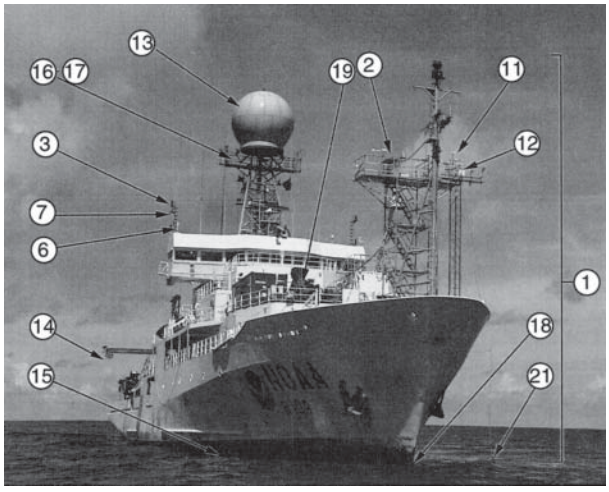

FIG. 2. Principal platform used in the first two phases (Apr and May 1999) of JASMINE was the NOAA research ship *Ronald H. Brown*. Numbers on the figure refer to the location of many of the instruments used during JASMINE and noted in Table 1. During the third phase of JASMINE (Sep 1999), the Australian research ship *Franklin* was deployed.

evident during the same period. However, during the second northward transect, the winds steadily increased in strength in both the upper and lower troposphere reaching gale force at the surface, which was maintained during star 2. Strong winds persisted for over 10 days as the intraseasonal event moved northward through the Bay of Bengal. Coincident with the increase of convection in the northern Bay of Bengal during star 2, the upper-tropospheric winds accelerated to speeds greater than 20 m s^{-1} and then intensified to 30 m s^{-1} during the last southward transect. The acceleration of the upper-tropospheric easterlies heralded the arrival of the monsoonal easterly jet stream for the 1999 summer monsoon. An intraseasonal component to the strength of the easterly jet stream is also apparent.

Figure 6 shows that during 12–15 May 1999 (star 1), the surface pressure gradients were slack prior to the onset of the southwest monsoon and only scattered low-level cumulus were observed from the *Brown*. During 22–25 May (star 2), the southwest monsoon commenced as the monsoon intraseasonal oscillation moved northward. The surface pressure gradient became very tight and strong cyclonic surface wind shear existed over the entire Bay of Bengal. The flow was essentially southwesterly and possessed a strong ageostrophic component toward the low pressure trough located in the northern Bay of Bengal. Deep clouds covered most of the bay.

Upper-ocean structure. A major goal of JASMINE was to determine the variability in the upper-ocean fields that occur during the intraseasonal transitions of the monsoon in the Bay of Bengal sector. Schott and McCreary (2001) provide a comprehensive review of monsoon circulation based on earlier observations and modeling studies. The Bay of Bengal sector of the Indian Ocean has been poorly sampled until recently. Murty et al. (1992) provide unique results based on a coarse array of temperature and salinity observations within the Bay of Bengal during the southwest monsoon. Bhat et al. (2001) report on the recent BOBMEX observations during July and August 1999. Bhat et al. (2001) and Sengupta and Ravechandran (2001) show the importance of the intraseasonal signal in this region. The upper-ocean observations during JASMINE are the first direct observations of the combined temperature, salinity, and velocity fields in the equatorial and southern Bay of Bengal regions of the eastern Indian Ocean during the onset of the southwest monsoon. These data also complemented the much earlier work during INDOEX (Schott 1976; Swallow 1980) that looked at the near-equatorial transition with the onset of the monsoon.

JASMINE documented strong intraseasonal variability of upper-ocean temperature, salinity, and velocity. Energetic zonal jets reversed over periods of weeks. The temperature and salinity fields and their associated mixed- and barrier-layer structures responded to intraseasonally varying currents and air–sea fluxes.

During April (phase I) strong eastward near-equatorial currents between 5°S and 7°N had peak speeds near 1 m s^{-1} (Fig. 7a). Some 25 days later (phase II), the zonal currents had reversed direction over nearly the entire section with peak near-equatorial westward flow of 0.8 m s^{-1}. By the time of the last transect of phase II in May, the currents near the equator had reversed again. The strong flow to the east in April is

FIG. 3. Three phases of the field phase of JASMINE showing the cruise paths in Julian days. (a) Phase I was made up of transects along 89 E. (b) In phase II, transects along 89°E were accompanied by two on-station periods, each five days in duration, where star patterns were executed (star 1 and 2, see inset). The location of the star surveys was changed from 5°N inthe original plan (Fig. 2) to be located in the fresher water pool to study its effect on mixed layer and barrier-layer evolution. Each star pattern was designed to take 18 h so that about six circuits were completed during each 5-day period. (c) During phase III, the Australians executed triangle maneuvers (see inset) each taking 8 h following a floating buoy drogued in the upper ocean. During the cruise, CTD casts and upper-atmosphere radiosonde

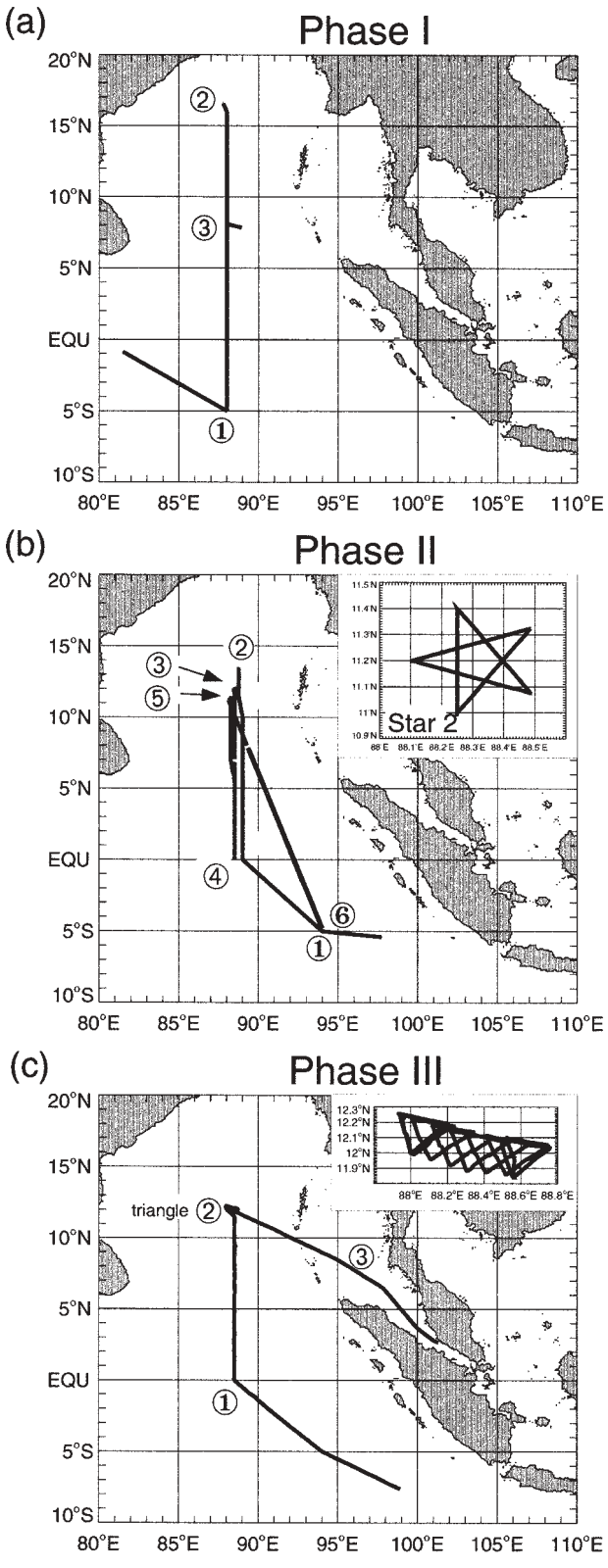

measurements were made. The number of these observations by phase is recorded in Table 2. All other instruments described in Table 1, or shown in Fig. 1, were run in continual mode. Way points are noted in the figure and cross-referenced to Table 3.

OBSERVATIONS DURING JASMINE

TRANSECT PERIODS

- ADCP velocity profiles at 1-km horizontal resolution.
- CTD stations to 1000 m at whole degrees and to 500 m at the intervening 1/2° intervals. At each station the ship was positioned to optimize eddy correlation flux estimates to correct for distortions (Edson et al. 1998) and mean meteorological and SST measurements were gathered to compute turbulent fluxes (Fairall et al. 1996; Chang and Grossman 1999) that were compared with the accurate direct covariance flux measurements.
- Continuous longwave and shortwave radiative fluxes monitoring.
- Continuous Doppler radar measurements at 3 GHz and 915 MHz to resolve mesoscale phenomena.
- Circulation structure: radiosonde measurements (6 times per day on the *Brown*; 4 times per day on the *Franklin*) at internationally agreed to times for upper-atmosphere soundings.

All other instrumentation operated in continuous mode.

STAR AND TRIANGLE PERIODS. The star periods needed to be large enough to sample the horizontal gradients associated with the dominant advective processes, yet needed to be completed in a short time compared to important periods of variability. The legs of the star were 44.4 km long with stations every 14.8 km. The circuit took about 18 h to complete, with a circuit around the inner pentagon of stations every 9 h. This circuit time was short compared to the inertial period at 10°N and minimized diurnal biases over the 5-day period.

The *Franklin* took 8 h to make its triangle (see Fig. 3). Experience in the equatorial east Indian Ocean (Godfrey et al. 1999) had shown this pattern to be effective in upper-ocean budget closure experiments. The triangle and star periods took place in the same region.

Measurements during these on-station observation periods:

- CTD station frequency increased to 14.8-km spacing with about 15 on-station observing periods for all parameters (atmospheric, air–sea flux, and oceanic) on the star, six CTD casts on the triangle.
- Upper-air soundings: remained four per day on the *Franklin*; increased to eight per day on the *Brown*. All other measurements on the same schedule as during the transects

All other instrumentation operated in continuous mode.

Table 2. Total number of upper-atmosphere soundings and CTDs by phase and leg. Overall 272 radiosonde ascents and 388 CTD casts were made during the 52 days of JASMINE.

PHASE	SECTION	SONDEs	CTDs
PHASE I:	Transects 1,2	23	44
PHASE II:	Transects 1,2,3,4 Stars 1,2	108 (at 6 day^{-1}) 85 (at 8 day^{-1})	124 103, 97
PHASE III:	Transects 1,2 Triangle	32 (1 day^{-1} for 8 days and 4 day^{-1} for 6 days 28 (4 day^{-1})	20 CTD plus 22 XBTs 126

Table 3. Three phases of JASMINE showing the dates of the north–south transects and their way points. During phase II and III there were periods were the ship remained on station executing maneuvers around a specific point for a number of days. These are referred to as stars or triangles, depending on the shape of the maneuver. The NOAA research ship *Brown* was the principal research platform used during phases I and II. The Australian CSIRO research ship *Franklin* was used during phase III. Numbers in the right-hand column refer to way points in Fig. 3.

PHASE	SECTION	DATES 1999	WAY POINTS	FIG. 3
PHASE I: Male–Singapore 7–22 Apr *Ronald H. Brown*	 Transect 1 Transect 2	 10–16 Apr 16–18 Apr	 4.8°S–88.0°E, 16.3°N–88.0°E 15.7°N–88.0°E, 8.0°N–88.0°E	 1–2 2–3
PHASE II: Singapore–Darwin 1 May8 Jun 1999 *Ronald H. Brown*	Transect 1 Star 1 Transect 2 Transect 3 Star 2 Transect 4	5–10 May 10–15 May 15–18 May 18–21 May 21–26 May 26–30 May	5°S–89.0°E, 13.5°N–88.8°E 11.9°N–88.6°E 11.6°N–88.5°E, 0°N–86.5°E 0°N–88.5°E, 11°N–88.2°E 11.2°N–89.3°E 11.2°N–88.1°E, 5°S–94.0°E	1–2 3 3–4 4–5 5 5–6
PHASE III: Darwin–Singapore 2–28 Sep *Franklin*	 Transect 1 Triangle	 12–16 Sep 16–23 Sep	 0.5 S–88.5 E, 11.5 N–88.5 E 11.7 N–88.7 E, 11.2 N–89.8 E	 1–2 2–3

consistent with the spring equatorial jet described by Wyrtki (1973) and with model simulations that interpret the jet as a Kelvin wave response to wind forcing (Han et al. 2001; Han et al. 2002, unpublished manuscript, hereafter HWHL). The strong flow to the west near the equator during most of May 1999 is opposite to the climatological equatorial jet (Wyrtki 1973). However, the near-equatorial surface current variability is almost certainly the result of the intraseasonal oscillation of the lower-tropospheric wind field. HWHL have managed to reproduce many aspects of the near-equatorial current field observed during JASMINE using ECMWF wind forcing.

The temporal variability of the temperature and salinity fields near the equator is, in large part, the result of the energetic changes in the near-equatorial velocity field. The top of the thermocline is fairly well represented by the 28°C isotherm, which is near a depth of 100 m at the equator and shoals to about 50 m in the vicinity of 10°N within the Bay of Bengal. The layer above the 28°C isotherm contains both the mixed layer and the barrier layer (Lukas and Lindstrom 1991). The temperature structure in Fig. 7b shows large changes in the depth of the top of the thermocline. The changes are consistent with geostrophic adjustment associated with the reversal of the zonal currents. The largest isotherm depth changes occur near 5°S and 5°N with the 25°C isotherm varying between 50 and 150 m (HWHL). The large changes in the thickness of the surface layer

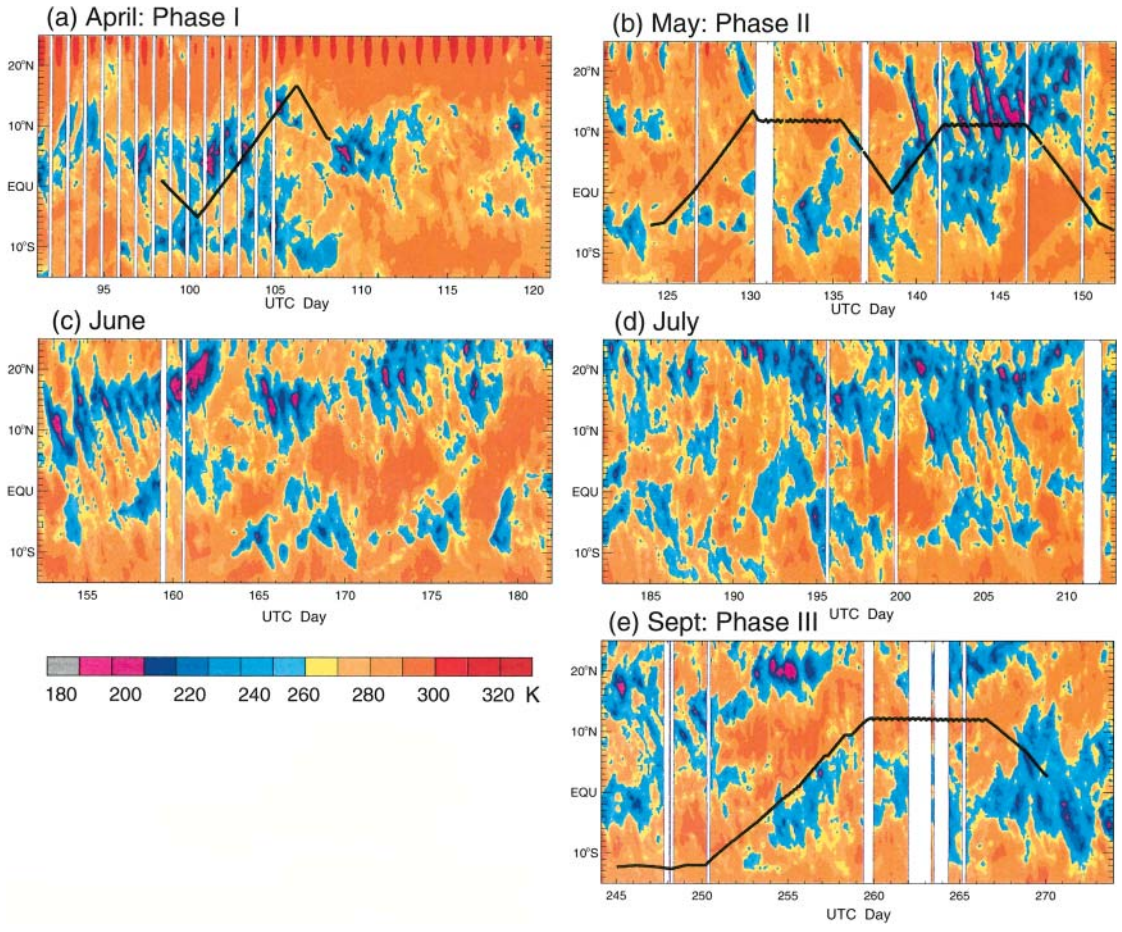

FIG. 4. Time–latitude sections of brightness temperature (see color-coded scale) from the European Space Agency *METEOSAT-5* geostationary satellite (a) Apr, (b) May, (c) Jun, (d) Jul, and (e) Sep of 1999. All sections are averaged between 85° and 90°E. Ship tracks for phases I, II, and III are shown in (a), (b), and (e), respectively. Aug 1999 has been omitted because of poor data quality. Cold temperatures are indicative of high cloud tops while relatively clear periods appear as warm temperatures representing infrared radiation emitted at the surface, the moist boundary layer, or from low-tropospheric clouds.

(mixed layer plus barrier layer) above the top the thermocline are arguably the result of near-equatorial dynamics (Han et al. 2001; HWHL). Another interesting feature of the thermocline is the sharp vertical temperature gradient near the equator compared to the more diffuse thermocline structure farther to the north within the Bay of Bengal. The mixed layer depth varies from less than 1 to over 100 m depending on air–sea flux forcing and background ocean density structure. During JASMINE, the deepest mixed layers and thickest barrier layers were found within 6° of the equator with barrier layer thicknesses of the order of 100 m near the equator during low wind conditions.

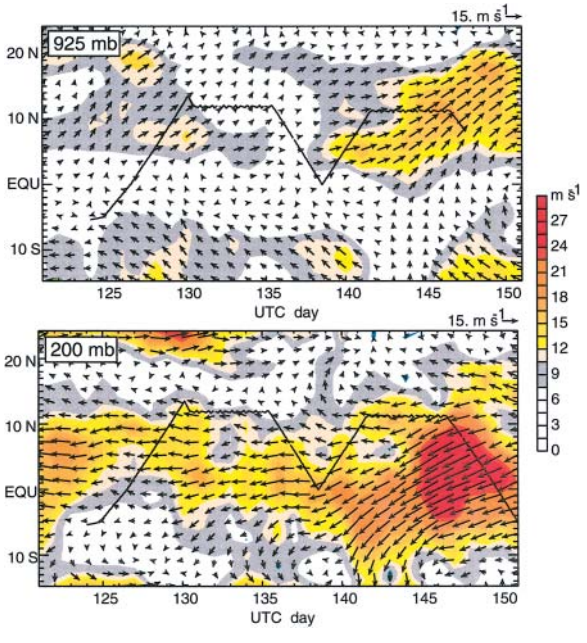

FIG. 5. Daily averaged (top) 925- and (bottom) 200-mb vector winds from ECMWF along 89°E for phase II of JASMINE. Color coding denotes wind speed relative to the scale to the right of the panel.

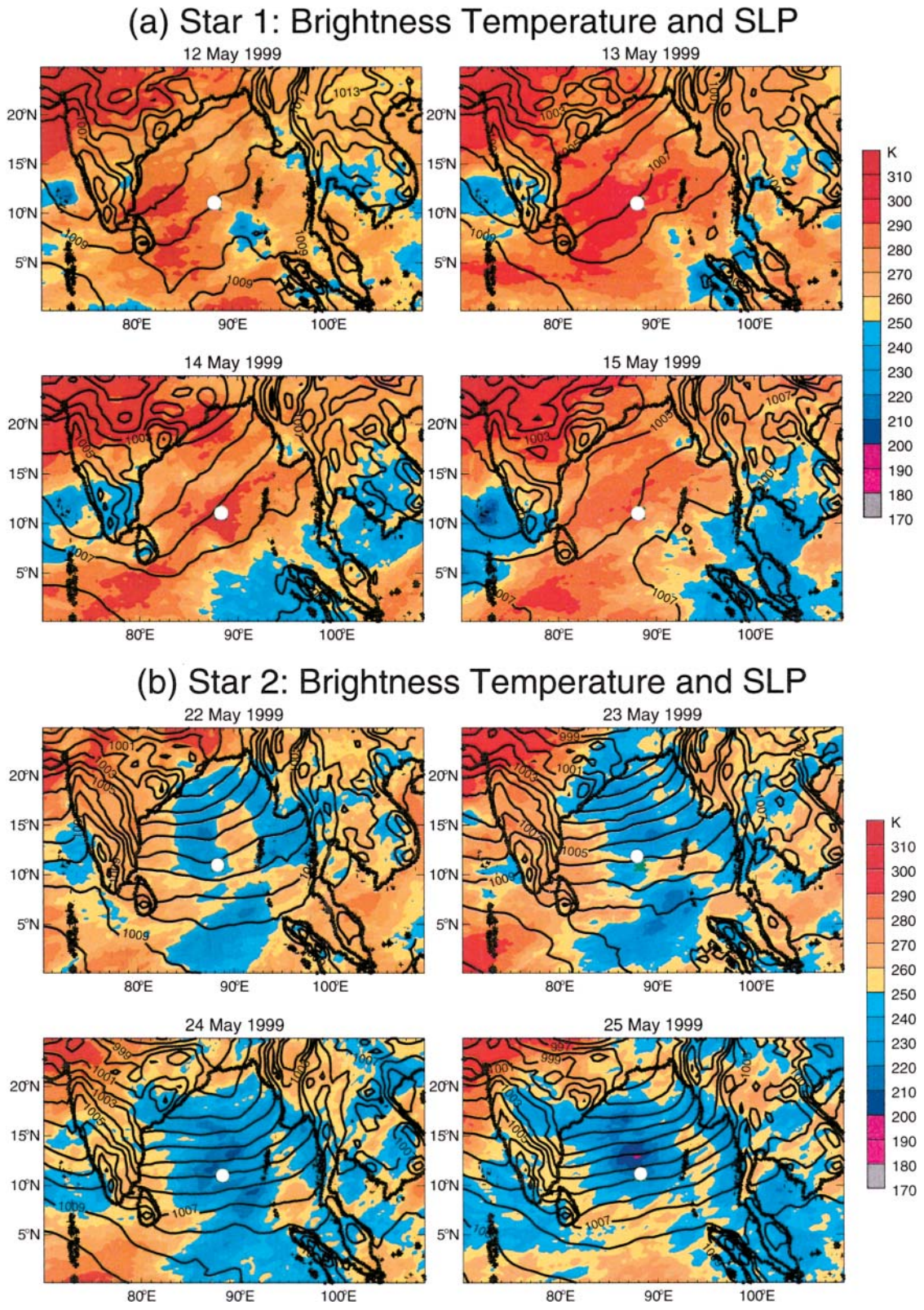

FIG. 6. (a) Synoptic situation during star 1 of JASMINE. Both 24-h-average brightness temperature and surface pressure fields are shown for the period 12–15 May 1999. The period is highlighted by weak surface winds and strong insolation. (b) Same as (a) except for the disturbed and convective star-2 period during 22–25 May 1999. The white dot denotes the location of the *Brown*. The isobaric analysis is from ECMWF and the brightness temperature is from the European Space Agency *METEOSAT-5* geostationary satellite.

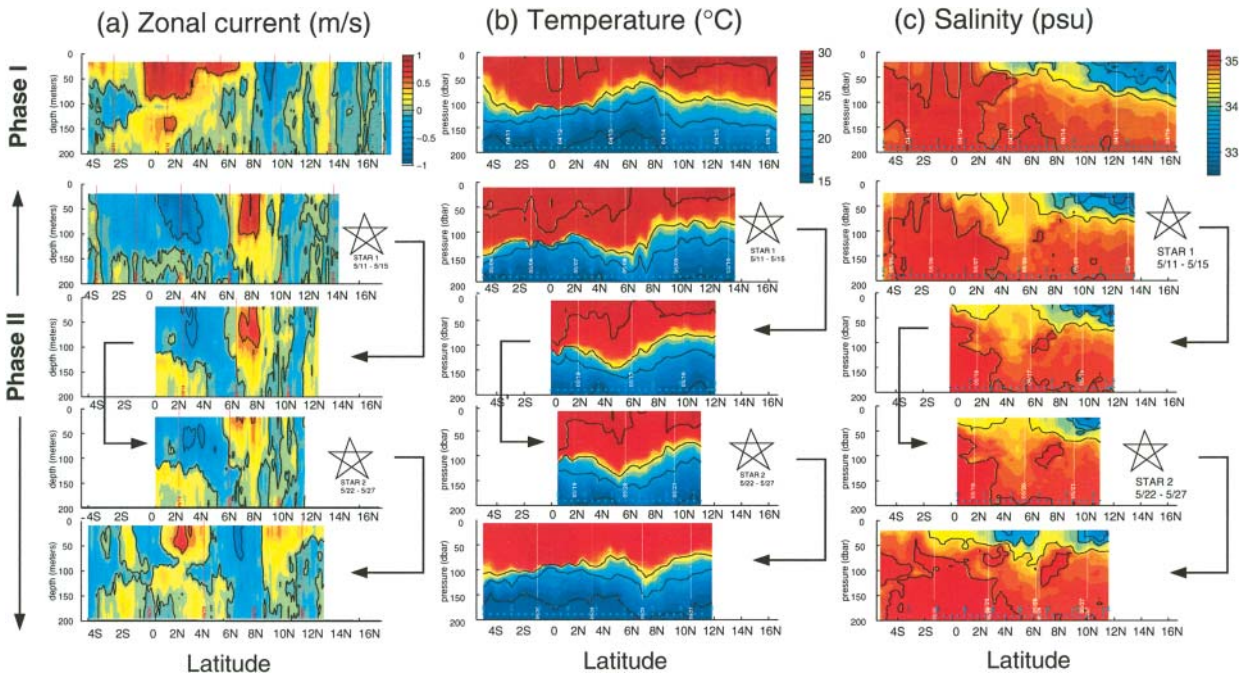

FIG. 7. (a) Zonal current (m s^{-1}) of the upper ocean for the five transects of phases I and II of JASMINE, plotted as a function of depth and latitude. Vertical lines are 1 day apart. Sections are arranged from south to north and the arrows indicate the direction of the transects. The star patterns indicate the time of the on-station budget surveys conducted near the northern end of the transects, to the north of the freshwater front. Note the reversal of zonal current with latitude. Near the equator, the zonal current reverses direction twice, going through a complete oscillation in a 50-day period. Overall, the ocean currents show a strong intraseasonal oscillation. Solid lines show 1.0, 0.5, 0, –0.5, and –1.0 m s^{-1} contours. (b) Same as (a) except for the temperature structure (°C). Solid lines indicate 15°, 20°, 25°, and 30°C contours; (c) same as (a) except for salinity (psu). Solid lines indicate 33.5-, 34.0-, 34.5-, and 35.0-psu contours. Note the large difference in the salinity between the northern and southern ends of the Bay of Bengal.

The strong zonal jets and thick barrier layers suggest that salinity appears to be critically important to ocean dynamics in the eastern Indian Ocean. Similar conclusions can be reached from the modeling results of Masson et al. (2002). Thus salinity needs to be observed systemically and included in upper-ocean model simulations. The primary feature in the upper-ocean salinity structure along the five transects (Fig. 7c) is the freshwater front located near 8°–10°N (Hacker et al. 1998; HWHL). In historical data, the front extends from the southeast toward the northwest in the eastern Bay of Bengal. Each section in Fig. 7c shows a detached blob of fresher water to the south of the main freshwater pool. The observations suggest either a convoluted frontal structure or the advection of freshwater blobs away from the frontal boundary. The front appears to be a horizontal stirring region between the fresher water to the north and the saltier water to the south, and it affects local upper-ocean mixed layer and barrier layer structure as well as temperature and salinity. While these layers were as deep as 100 m near the equator, the deepest mixed and barrier layer thicknesses north of the front were typically 30–40 m during phases I and II of JASMINE.

During the undisturbed star 1, waters above 30 m show a net warming and freshening (Fig. 8a). The warming is consistent with the net air–sea heat flux data, but the freshening is inconsistent with the observed net evaporation. Preliminary calculations indicate the importance of horizontal advection in the local heat and salt budgets, and suggest that the observed evaporation is correct but overshadowed by advection of freshwater into the survey domain. The cycle of diurnal heating and cooling is also apparent: The deepest mixed layers (about 40 m) during star 1 occur during the nighttime cooling, and the shallowest mixed layers and the thickest barrier layers (about 30 m) occurred during the day.

Figure 8b shows a net cooling and freshening above 30 m during the active star-2 period. In this case the cooling and freshening are consistent with a net heat flux out of the ocean and a net precipitation minus evaporation flux into the ocean. The diurnal cycle is

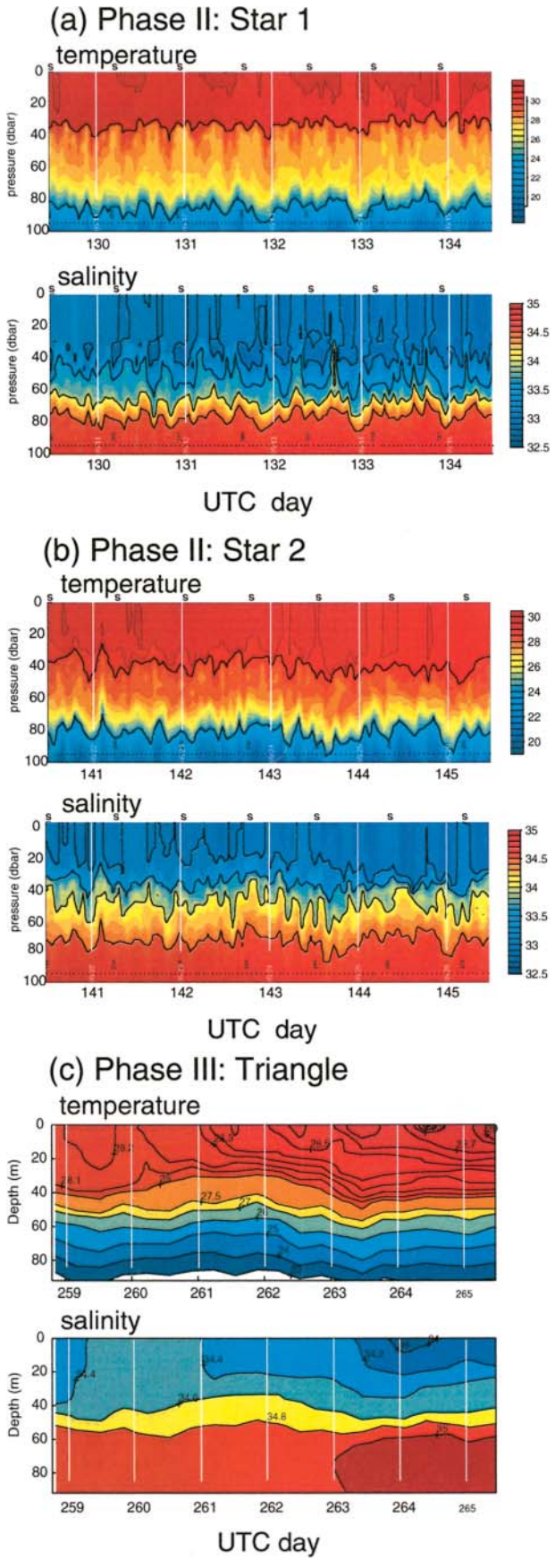

only weakly apparent during the first two days of star 2. The mixed layer deepens linearly from about 20 to 40 m over the 5-day survey. The barrier layer is generally thinner during star 2 compared to star 1 with typical thicknesses between 0 and 20 m.

For both star 1 and star 2, which were conducted north of the freshwater front (see Fig. 7c), the salinity effect on density is critical and often dominates over the effect of temperature. This is apparent in Figs. 8a and 8b over the depth interval of 40–60 m just below the deepest mixed layers. Over that depth interval, the temperature changes by about 1°C while the salinity changes by 1 psu (practical salinity units). The effect of salinity on density is about 4 times as great as temperature in this region, per unit change.

The triangle survey of JASMINE phase III was conducted during an undisturbed period of net heat flux into the ocean and low net evaporation but also net freshening (Fig. 8c). As during star 1, preliminary budget calculations show that horizontal advection must be important. Another interesting result shown in Fig. 8c is that after four months of monsoon forcing the depth of the 28°C isotherm was still at about 40 m in the Bay of Bengal, the same as during star 2. The top of the thermocline has not deepened here. The data suggest that the strong salinity stratification may isolate the upper 40 m of the water column from the deeper layers during typical monsoon conditions within the freshwater pool in the Bay of Bengal. This has important implications for regional air–sea coupling, and could be related to the precipitation maximum in the Bay of Bengal.

Atmospheric structure. The top panel of Fig. 9a shows time–height sections of the winds and relative humidity for the star-1 and -2 periods. The lower panel shows the corresponding radar reflectivity separated into two intensity bands. Figure 9b shows the vertical distribution of the relative humidity, temperature difference, and winds in each star period. A brief comparison of JASMINE and the Tropical Ocean Global Atmosphere Coupled Ocean–Atmosphere Response

FIG. 8. (a) (top) Temperature and (bottom) salinity plotted as a function of depth for star 1. (b) Same as (a) except for star 2. Note cooling and deepening and slight freshening of upper 30 m. (c) Same as (a) except for phase III from the *Franklin*. Time in Julian (UTC) days. Vertical line denotes 0000 UTC of each day. Although the position of the ship varies during each of the surveys, the sections represent the space–time evolution of the fields plotted only as a function of time.

Experiment (TOGA COARE) atmospheric structures is given in section 4.

During star 1, the winds were relatively light throughout the column. Moist air was confined to the boundary layer where light southwesterlies persisted. There is little convection, although a thin cirrus cloud persisted during much of the period. The cirrus, although only barely discernible from the ship, was occasionally 2–5 km thick as indicated by the cloud radar. During star 2 the winds freshened to near-gale force. The strengthening of the southwesterlies below 400 mb and northeasterlies in the upper levels increased the negative vertical shear substantially throughout the troposphere. Individual winds in the upper troposphere had magnitudes > 30 m s^{-1}, while lower-tropospheric winds exceeded 20 m s^{-1} for considerable periods. Compared to star 1, the entire troposphere had moistened remarkably during the intervening week, accompanying the penetration of convection into the upper troposphere. Deep convection is an order of magnitude more abundant during the night than during the day during the disturbed period.

The aerological data from JASMINE indicates that the tropospheric structure changes significantly between the quiescent and disturbed phases of a monsoon intraseasonal oscillation. In the quiescent phases, the troposphere is remarkable dry above the boundary layer with weak upper-level easterly winds surmounting weak surface southwesterlies. During the disturbed phase, the entire troposphere becomes very moist and the weak wind structure is replaced by strong lower-level southwesterlies and upper-level northeasterlies.

Surface flux variability. One of the major objectives of the JASMINE pilot study was to document surface fluxes during an intraseasonal oscillation. A further objective is to ascertain the degree of similarity of surface fluxes between Indian Ocean and Pacific Ocean intraseasonal variability, the latter being described by Godfrey et al. (1998).

Two very different distributions of surface heat flux components were found in star 1 and 2 (Fig. 10 and Table 5). For example, net surface longwave radiation was 58% greater during star 1 than in star 2, due primarily to the more extensive low-level cloud, and to the increase of moisture found throughout the entire troposphere during disturbed periods (Fig. 9b). Instantaneous values of latent heat flux range from –50 W m^{-2} at times during star 1 to over –300 W m^{-2} during star 2 associated with the passage of a nocturnal gust fronts. Figure 11 shows the daily averaged net surface flux for phases I and II of JASMINE. Together with Table 1 it can be seen that there is a change from a net heating to a net cooling between disturbed and undisturbed periods. This reversal is the combined result of changes in solar radiation and evaporation. In general, a higher surface solar radiation is associated with a lower evaporative heat loss and vice versa. Furthermore, the sensible heat loss by the ocean due to turbulent transfer and rain cooling was not important during the undisturbed period, but became moderately important during star 2 when increased winds enhanced turbulence. Also, instantaneous values of the sensible heat loss due to rain cooling of the ocean surface were occasionally greater than –200 W m^{-2}. Overall, the differences in net surface flux between the two star periods were caused by a severe reduction in net surface radiation, and increases in the turbulent fluxes, although, offset slightly by a decrease in net longwave radiation loss. The changes in turbulent fluxes can be accounted for, to a large degree, by the large increases in surface wind strength.

Diurnal variability. One of the general characteristics of the tropical atmosphere is the strong diurnal variability of convection, SST, and surface fluxes as were noted, for example, in the western Pacific Ocean during TOGA COARE (Webster 1994; Weller and Anderson 1996; Webster et al. 1996; Godfrey et al. 1998) and in the Arabian Sea (Weller et al. 1999). The largest diurnal variability at the surface in the Pacific was observed during undisturbed periods when insolation was strong and the winds were light (Webster 1994). Comparing the two star periods for JASMINE, however, shows that, contrary to expectation, a surprising amount of diurnal variability exists during disturbed periods.

One of the striking features of the brightness temperature distribution in the Bay of Bengal is the extremely strong diurnal variability occurring during the disturbed period of phase II. This variability can be identified as southward-propagating deep convection with nocturnal maxima. Sections for June and July (Figs. 4c,d; detail shown later in Fig. 14) indicate similar diurnal disturbances are present during each disturbed phase of a monsoon intraseasonal oscillation.

During star 1, maximum values of SST and air temperature occur in late afternoon. During the disturbed star-2 period, the SST shows little or no diurnal variability although the air temperature varied considerably (Fig. 12). The nocturnal cooling of the boundary layer was caused by the convective downbursts associated with the nocturnal squall lines that propagated southward each night during star 2. Also during star 2, there were universally stronger surface

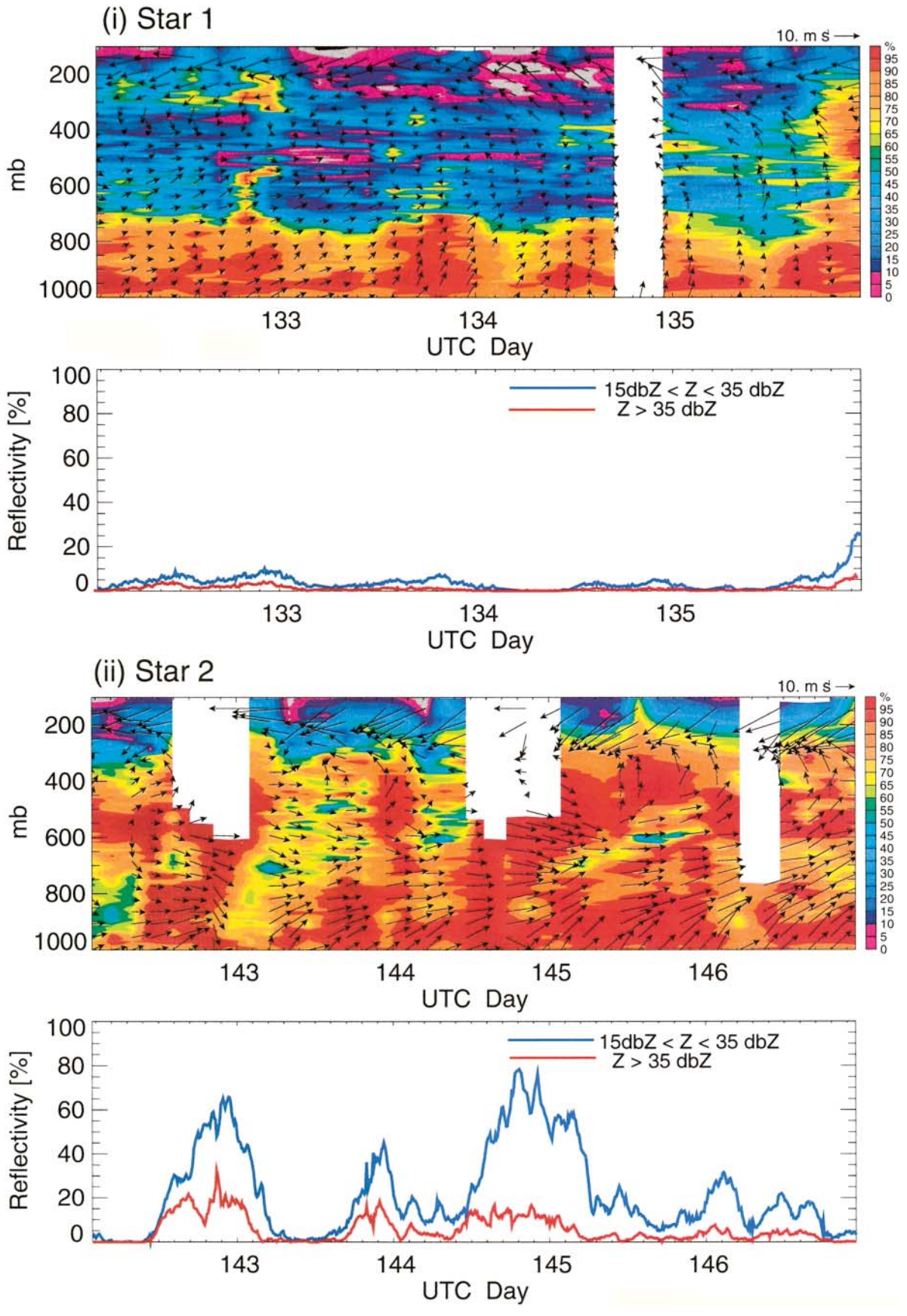
(i) Star 1
10. m s⁻¹
mb
200
400
600
800
1000
133
134
135
UTC Day
%
95
90
85
80
75
70
65
60
55
50
45
40
35
30
25
20
15
10
5
0
Reflectivity [%]
100
80
60
40
20
0
15dbZ < Z < 35 dbZ
Z > 35 dbZ
133
134
135
UTC Day
(ii) Star 2
10. m s⁻¹
mb
200
400
600
800
1000
143
144
145
146
UTC Day
%
95
90
85
80
75
70
65
60
55
50
45
40
35
30
25
20
15
10
5
0
Reflectivity [%]
100
80
60
40
20
0
15dbZ < Z < 35 dbZ
Z > 35 dbZ
143
144
145
146
UTC Day

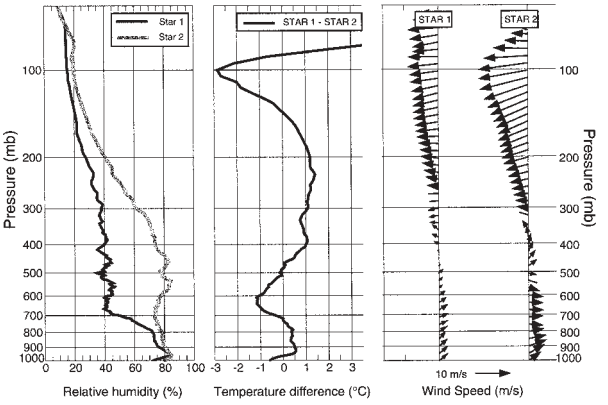

FIG. 9. A more detailed view of the convective and dynamic structure of the atmosphere compared to Figs. 4 and 5. (a) Time–height sections of horizontal wind (vectors: m s^{-1}), relative humidity (%) (top panels), and radar reflectivity (bottom panels percent with values 15 dBZ < Z < 35 dBZ in blue and Z > 35 dBZ in red) for (i) star 1 and (ii) star 2. During the undisturbed period (star 1) the mid- and upper troposphere is extremely dry. Little convection beyond trade cumuli existed at this time. During the disturbed period (star 2) the mid- and upper troposphere has markedly moistened, stronger winds prevail throughout the column and convection is deeper and stronger. Note the marked nocturnal maximum in the convection. Time in Julian (UTC) days. The two radar reflectivity curves show the percent area within 100 km of the *Brown* with reflectivity in the range of 15–35 dBZ (blue curve) and > 35 dBZ (red curve). (b) (left) A comparison of the mean vertical relative humidity distribution (%) for star 1 (black) and star 2. (middle) The vertical distribution of the mean temperature differences(°C) between the two star periods. (right) The mean vertical wind distributions for star 1 and star 2.

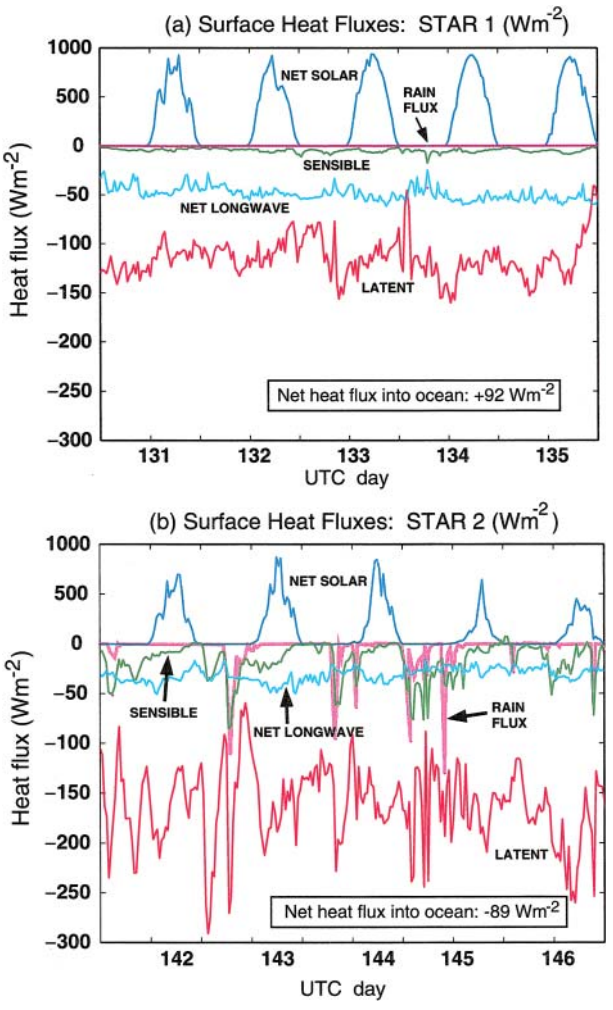

FIG. 10. Components of the surface energy balance (W m^{-2}) for (a) star 1 and (b) star 2. Five surface fluxes are shown: the solar radiative flux, sensible turbulent heat flux, latent turbulent heat flux, net longwave flux (outgoing surface minus incoming atmospheric), and the sensible heat flux of rainfall. Units: W m^{-2}.

winds with larger variability at night (not shown) but associated with the recurring surges that were apparent in the latent heat fluxes shown in Fig. 10b. However, most evident is the very strong nighttime maximum in rainfall rate. Again, the nocturnal maximum is associated with the propagating disturbances.

The latent heating (LH) distributions (Fig. 13a) largely follow the mean diurnal variation of the winds (Fig. 12b), as does the variation of the sensible heat (SH). However, the latter flux is enhanced during star 2 by the strong nocturnal decrease in 10-m air temperature. The solar radiation is severely reduced and the downwelling infrared radiation is higher during the disturbed period. Very strong negative surface shortwave forcing is apparent in the star-2 period during the daytime because of the generally overcast conditions during the disturbance.

Large-scale convection. The nocturnal convection appeared to have a form that was unique to the region with strong propagating convective bands that moved southward from the head of the Bay of Bengal in directions orthogonal to the wind direction at all levels. These propagating disturbances severely perturbed the surface fluxes as they propagated southward past the ship (Fig. 10). Furthermore, there is evidence that the propagations continued into the Southern Hemisphere as far south as 10°S (Figs. 4 and 14). Along a track, the amplitude of the convection appears to decrease during the next local daytime but grows once again farther to the south during the following night.

During each of the intraseasonal events occurring throughout the summer of 1999, propagations of diurnal signals are evident along trajectories of 2000–3000 km in length with propagation speeds in the

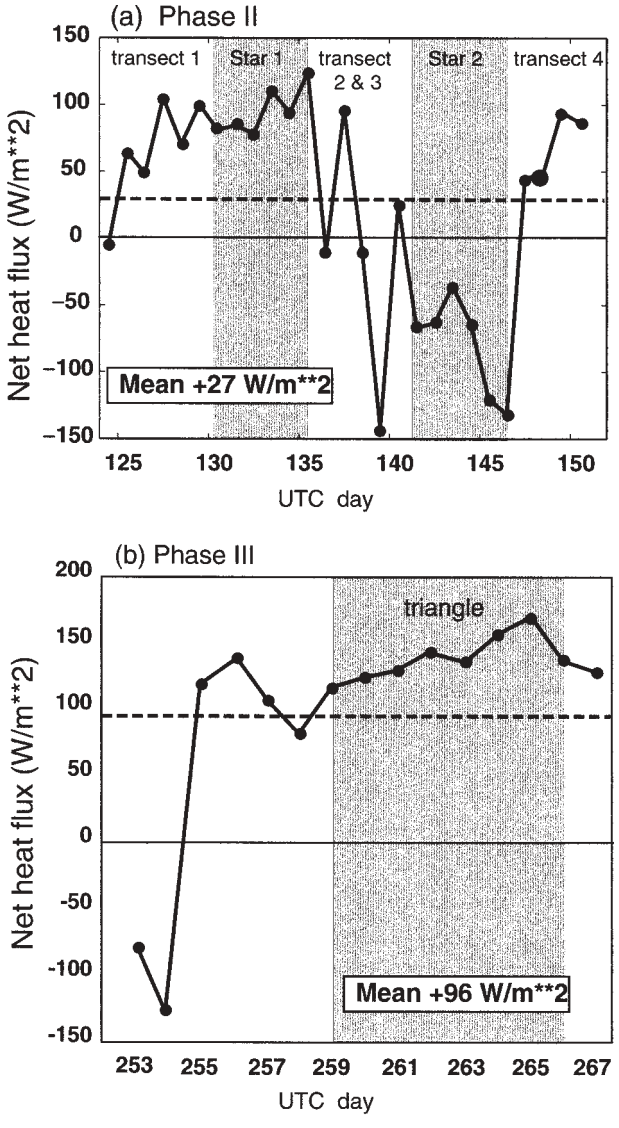

FIG. 11. Daily averaged net heat flux into the ocean during (a) phase II and (b) phase III. The shaded areas indicate the on-station star patterns (phase II) or the triangle patterns (phase III). Units: W m^{-2}.

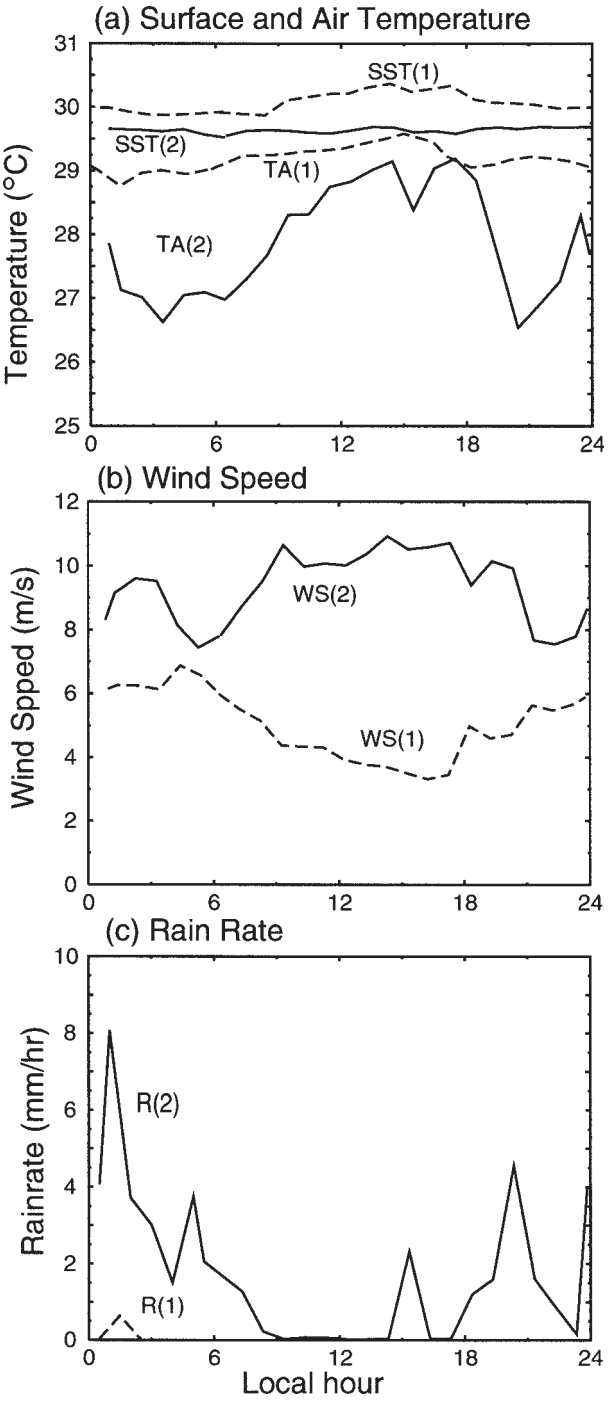

FIG. 12. Average diurnal variability of the (a) sea surface and 10-m air temperature (SST, TA: C), (b) surface wind speed (WS: m s^{-1}), and (c) rain rate (R: mm h^{-1}) for star 1 (dashed lines) and star 2 (solid lines).

range 50–60 km h^{-1}. The convective disturbances usually formed in the early afternoon over the land areas in the northern reaches of the Bay of Bengal (Zuidema 2003, hereafter Z03). The disturbances adopt a southwest–northeast orientation roughly parallel to the surface isobars (Fig. 6b) and extend 300–500 km. In the direction normal to propagation (perpendicular to the wind), the disturbances are much narrower with scales of about 50 km. Quite probably these features have characteristics of propagating gravity waves. Using a multiyear global cloud archive, Yang and Slingo (2001) find persistent diurnal propagations in the Bay of Bengal with convection commencing over the land at the head of the Bay. These features and their ubiquity as a component of disturbed conditions in the Bay of Bengal has been confirmed by Z03 who studied other years in addition to 1999. Prior to JASMINE, however, and the subsequent papers of Yang and Slingo (2001) and Z03, these vigorous diur-

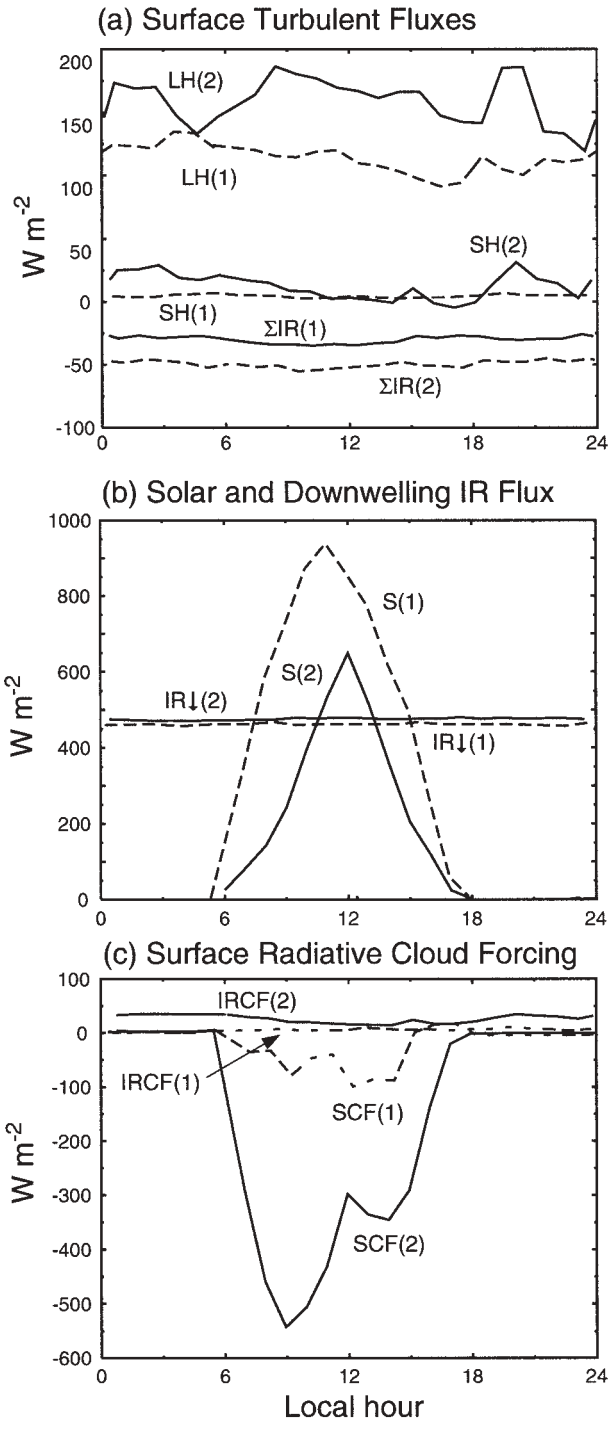

FIG. 13. Diurnal variation of the surface fluxes between the atmosphere and the ocean for the periods of star 1 (dashed) and star 2 (solid): (a) the surface turbulent fluxes and the net longwave radiation, (b) the solar and downwelling longwave radiation, and (c) calculations of the diurnal variability of the shortwave and longwave surface cloud forcing. Units: W m^{-2}.

nal convective events do not appear to have been documented.

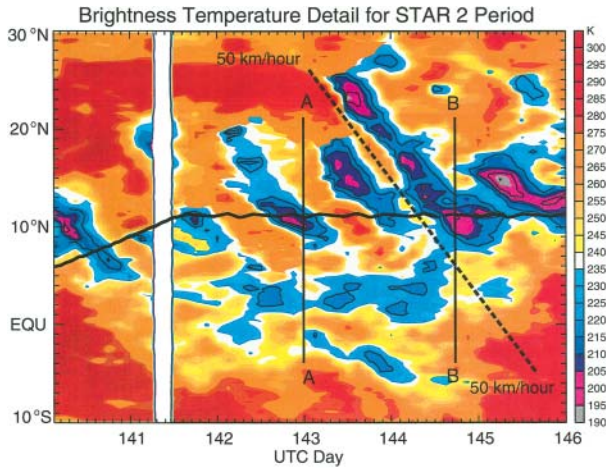

FIG. 14. Detail of the brightness temperatures (K) plotted as a function of latitude and time with twice the resolution of Fig. 4b. Sloping lines represent phase lines of 50 km h^{-1}. A–A and B–B refer to convective events shown in Figs. 15 and 16. Time in Julian days (and in UTC) is shown on the abscissas. The relationship of Julian days and UTC is such that day 142.00 corresponds to 22 May at noon or 221200.

In between the nocturnal episodes of deep, intense convection that passed the *Brown* each evening are extensive, deep nimbostratus decks. These may be seen in the cloud radar data shown in Fig. 15. The time–height sections encompass the passage of two nocturnal convective events demarked in Fig. 14 by the lines A and B. Cloud radar signals are attenuated very rapidly with deep convection and rain but the sections provide an indication of the broadscale stratiform clouds that accompany the disturbances. Figure 16 shows examples of the C-band radar data obtained during the passage of the same two disturbances. Broad bands of deep convection within the larger-scale mesoscale convective system are evident in the figures. To a large degree, these two JASMINE systems appear to be similar to the "superconvective" systems defined by Chen et al. (1996) for the western Pacific Ocean. Parts of the convective systems had developed stratiform precipitation over the ship [Figs. 16a, (i)] on 23 May. On the other hand, the superconvective system of 24 May (Fig. 16b) was in a highly convective stage and had yet to produce an extensive stratiform region. The convective cells were deep and intense with echo top heights of at least 18 km [Fig. 16b, (ii)]. On this day, the 30-dB*Z* echo reached to 11 km and the radial velocity perturbations associated with these cells [Fig. 16b, (iii)] were also strong with speed differences of 5 m s^{-1} between the inside and the outside of the convective cells.

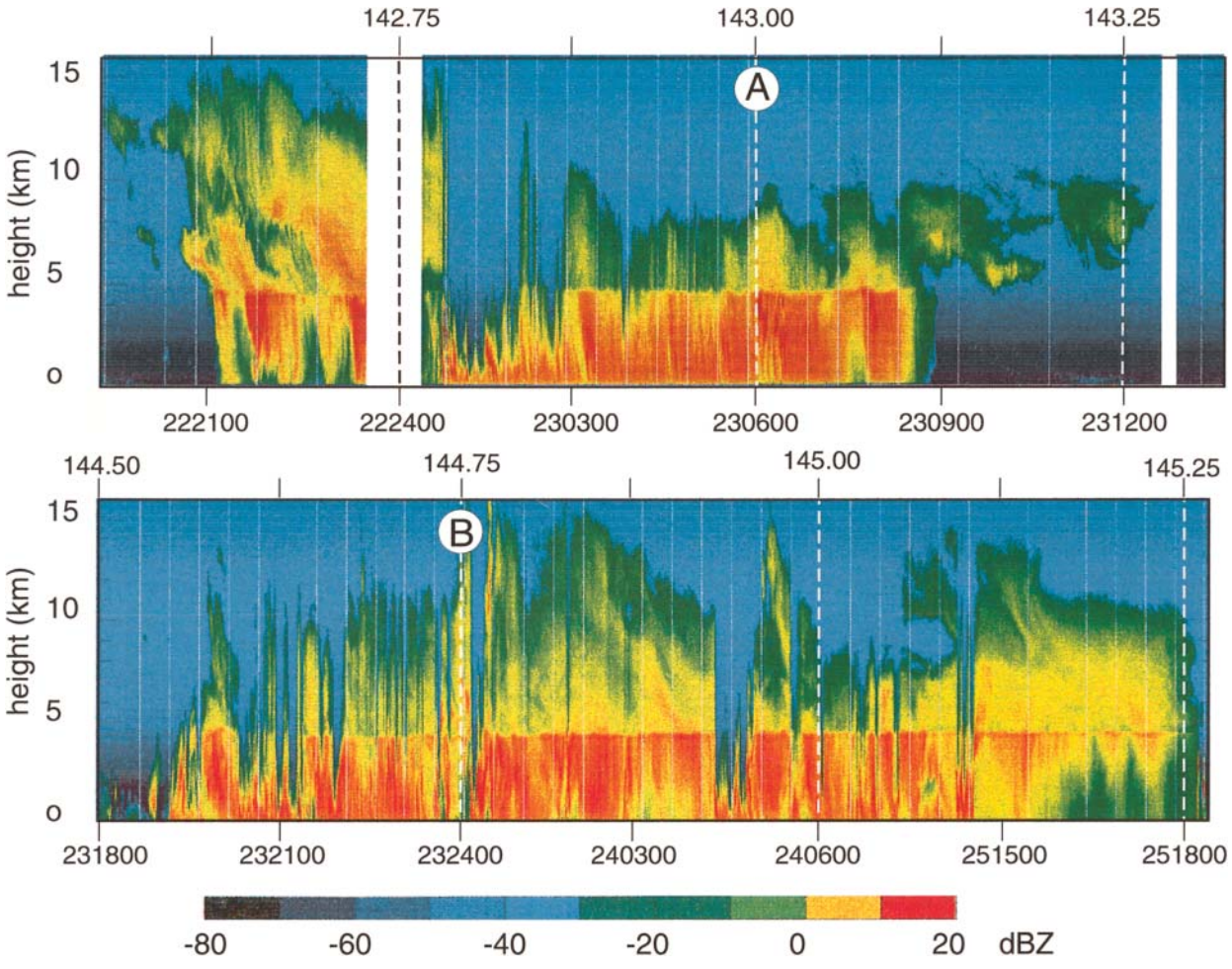

FIG. 15. Height–time sections of 35 GHz (K band) profiling "cloud radar" reflectivity between 1200 UTC 22 May 1999 and 1200 UTC 25 May 1999 during the star-2 period. Lines A and B correspond to same time as lines in Fig. 14. Both Julian days and UTC are indicated.

The C-band Doppler radar data collected during star 2 may suggest cooperative interactions between convection and the large-scale flow. The low-level momentum during star 2 was southwesterly, and not as strong as the northwesterly flow in the midtroposphere (Figs. 5, 9b, and 16a,b). The downward momentum flux in the convective and stratiform regions evidently increased the westerly component speed and made the wind veer slightly. As a result, the large-scale westerly component was accelerated by the convection, and low-level convergence with the ambient southwesterly component was created to generate still more deep convection. In the stratiform region there is a midlevel layer of northwesterly momentum flowing into the system between the 4- and 8-km level, where the environmental wind was strongly northwesterly as shown in Fig. 9. Doppler wind data shows inflow sloping downward, transporting the strong northwesterly flow toward the surface.

CONCLUSIONS, QUESTIONS, AND PLANS FOR FURTHER RESEARCH. A number of tentative conclusions are summarized below.

1) The surface flux data collected during JASMINE allows a comparison of the manner in which the atmosphere and ocean interact during active and break periods of the monsoon. Table 5 summarizes the flux data collected during JASMINE and also lists similar data collected during TOGA COARE.

   - During undisturbed periods (star-1 period and phase III), there was substantial heating of the ocean with average flux values of $> +90$ W m^{-2}. The heating during the undisturbed phase is in stark contrast to the strong cooling that occurred during the active phase (star-2 period) of the JASMINE pilot study when average fluxes were nearly -100 W m^{-2}. Given the limited

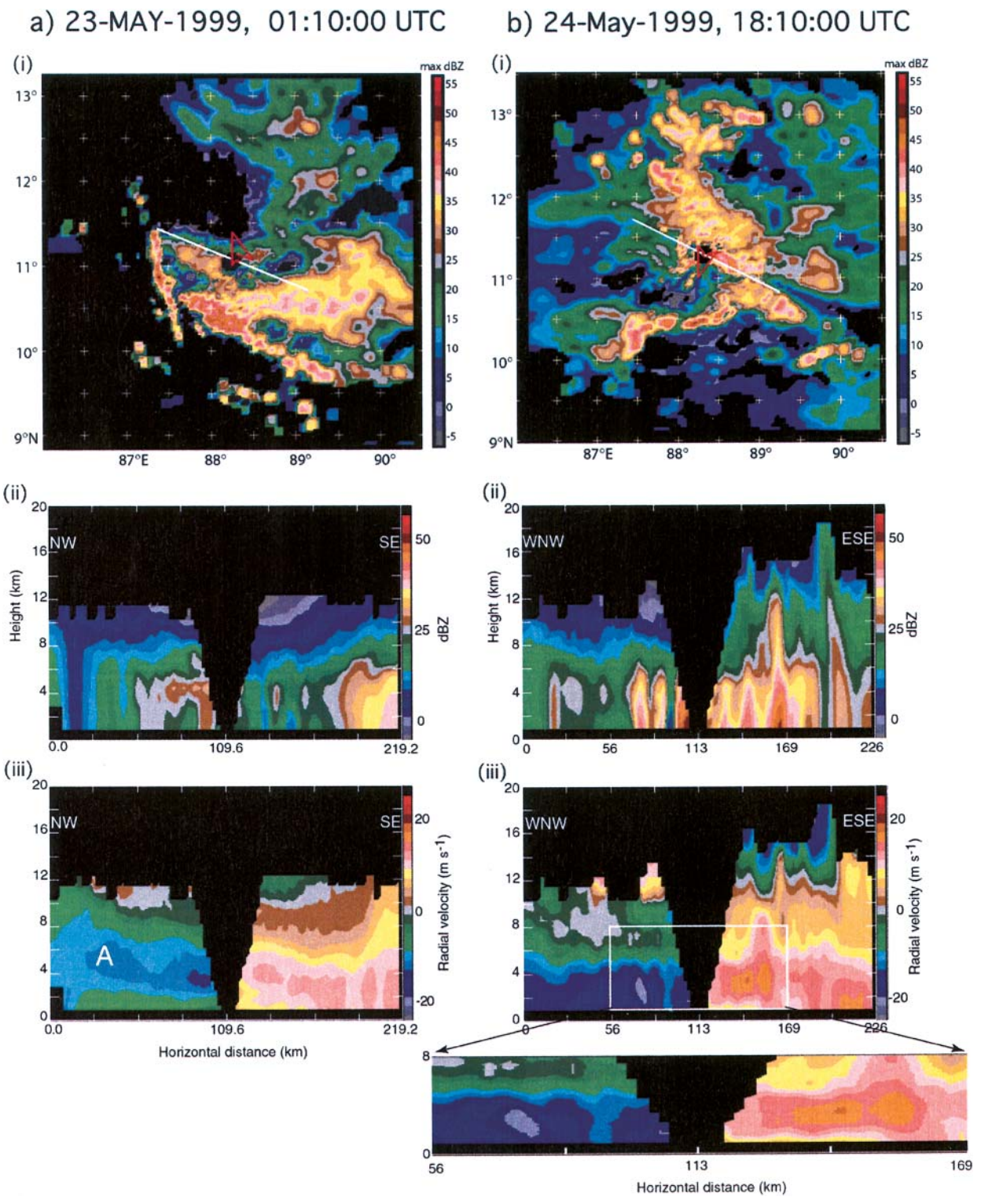

FIG. 16. C-band Doppler radar depictions of disturbed conditions on (a) 0110 UTC 23 May 1999, and (b) 1810 UTC 24 May 1999. The times of scans are marked as A–A and B–B on Fig. 14 and A and B on Fig. 15, respectively. For each situation, three sections are shown: (i) reflectivity as a function of latitude and longitude (dBZ), (ii) cross section of reflectivity (dBZ) along the white line marked in (i), and (iii) radial wind speeds along the white line (m s^{-1}) as determined by the Doppler radar. In (b), a section of the lower troposphere has been expanded.

Table 4. Comparison of average conditions of active and break periods in the Bay of Bengal compared to conditions during star 1 and 2. Comparisons are made with OLR (W m^{-2}) and 1000-mb wind speed (m s^{-1}). There were 59 active and 49 break periods used in compiling the climatology using criteria described in the text. NCEP reanalysis wind dataset was used.

	Break periods (49 events)	STAR 1	Active periods (59 events)	STAR 2
OLR (W m^{-2})	242 ±17	253	167 ±16	140
1000-mb wind speed (m s^{-1})	7.6 ±2.3	4.5	10.1 ±4.8	9.9

duration of the JASMINE pilot study, it is difficult to say if these values are indicative of break and active periods of the monsoon. However, statistics compiled from reanalysis and satellite data (Table 4) suggest that conditions found in the star 1 and 2 may be representative of break and active periods.

- The TOGA COARE fluxes shown in Table 5 (measured from shipborne systems such as those deployed during JASMINE (Fairall et al. 1996) and from the Improved Meteorology (IMET) buoys (Weller and Anderson 1996)) also display great variability between active and undisturbed periods. The first TOGA COARE period (11 November–3 December 1992) was a relatively quiescent period with net flux of +65 W m^{-2}, while the second TOGA COARE period (16 December 1992–11 January 1993) contained one of the strongest westerly wind bursts recorded in the western Pacific Ocean. The net flux for this burst period was –12 W m^{-2} compared to –89 W m^{-2} during star 2. The third TOGA COARE period (28 January–16 February 1993) possessed above-average winds and showed a net flux of +13 W m^{-2} into the ocean. However, each of these three phases contained a mixture of disturbed and undisturbed periods and transitions between phases of intraseasonal oscillations. Thus, mean fluxes during TOGA COARE periods were calculated using the criterion of Johnson and Ciesielski (2000), which defined undisturbed days as having precipitation < 5 mm day^{-1} and disturbed days as having precipitation rates > 10 mm day^{-1}. In total, 35 undisturbed and 37 disturbed days were identified in this manner. In general, the undisturbed periods of TOGA COARE and JASMINE had very similar net

Table 5. Comparison of Indian Ocean fluxes obtained during JASMINE with those obtained in the western Pacific Ocean TOGA COARE. Mean surface flux data is listed for the three periods of TOGA COARE (11 Nov–3 Dec 1992, 16 Dec 1992–11 Jan 1993, and 28 Jan–16 Feb 1993). The TOGA COARE data was binned further into disturbed and undisturbed day using the criteria of Johnson and Ciesielski (2000). Flux data for phases II and III of JASMINE are shown together with the means for star 1 and 2."SOLAR," "LW," "SEN," "LH," "RAIN," and "NET" refer to the net solar radiation, the net longwave radiation, the sensible and latent turbulent heat fluxes, the sensible heat flux due to rain, and the net flux at the surface, respectively. Units: W m^{-2}.

EXPERIMENT	SOLAR	LW	SEN	LH	RAIN	NET
PACIFIC						
TOGA COARE (TC) Pilot	+197	–43	–12	–116	–3	+22
TC period 1	+222	–58	–7	–89	–1	+65
TC period 2	+166	–46	–11	–117	–4	–12
TC period 3	+190	–51	–10	–112	–3	+13
TC undisturbed	+247	–57	–5	–84	–1	+99
TC disturbed	+158	–43	–11	–150	–5	–51
INDIAN						
JASMINE phase II	+205	–43	–9	–125	–2	+27
Phase II: star 1	+260	–49	–5	–115	–0	+92
Phase II: star 2	+128	–31	–17	–162	–7	–89
JASMINE phase III	+229	–38	–3	–92	–1	+96
Average TOGA COARE	+198	–49	–8	–105	–3	+34
Average JASMINE (II+III)	+217	–42	–6	–109	–2	+62

surface heat fluxes with values > 90 W m^{-2}. Given the greater sampling of undisturbed days in JASMINE, a greater confidence can be attributed to this comparison. The disturbed periods of JASMINE showed a much stronger negative heat flux than disturbed periods during TOGA COARE principally because of the greatly reduced net solar flux at the surface. Because of the relatively few disturbed days in JASMINE, less confidence can be placed in this comparison. However, this uncertainty may be offset to some extent by noting the similarity of the wind and OLR characteristics of the star-2 period with other active monsoon periods (Table 5).

2) The JASMINE pilot study successfully observed the upper-ocean structure during active and break periods and during the transition between these periods.

   - Energetic jets and circulation features reversed in the upper ocean on intraseasonal timescales. Likewise, the temperature, salinity, and air–sea flux fields varied strongly on intraseasonal timescales.
   - A strong barrier layer exists in the Bay of Bengal. Large changes were observed in the thickness of the surface layer (mixed layer plus barrier layer) and these appear to be consistent with near-equatorial dynamics as suggested by Han et al. (2001; HWHL).
   - Upper-ocean observations indicate that realistic ocean models must include salinity as well as temperature, and must have high vertical and horizontal resolution to resolve mixed- and barrier-layer structure affecting SST.
   - The JASMINE observations help to provide a firm basis for the design of an ocean observing system and future process studies in the Bay of Bengal sector. The new upper-ocean observations add significantly to the historical regional database. The JASMINE data allows, for the first time, a detailed comparison between disturbed and undisturbed conditions in the warm pools of the Indian Ocean and the Pacific Ocean. A comparable dataset was collected during TOGA COARE (Feng et al. 2000).

3) The atmospheric sounding data collected during JASMINE provided the opportunity to compare the character of the atmosphere during active and break periods in the eastern Indian Ocean and also between similar periods that occurred during TOGA COARE. TOGA COARE disturbed and undisturbed fields were computed using the criteria of Johnson and Ciesielski (2000), described above.

   - In general, the atmosphere was considerably moister during active periods than break periods, especially in the mid- and upper troposphere (Fig. 9b). Winds speeds increased from about 4 to nearly 10 m s^{-1} near the surface between the undisturbed and disturbed periods. During the same period upper-tropospheric winds increased from about 15 to more than 25 m s^{-1}.
   - The vertical distribution of relative humidity during the disturbed periods of JASMINE and TOGA COARE appear to be very similar with averages in both locations of about 80% up to 400 mb. However, the relative humidities of the undisturbed periods of JASMINE are about 20% less than the undisturbed TOGA COARE periods with average humidities in the 700–300-mb layer of about 40% and 60%, respectively. Why the mid- and upper troposphere in the Bay of Bengal should be so dry during undisturbed periods is unknown.

4) The radar systems aboard the *Brown* allowed an unprecedented view of convection in the eastern Indian Ocean.

   - As in the Pacific warm pool region, propagating large-scale convective elements dominate disturbed periods amid deep stratiform environment. In both regions the convection possesses a nocturnal maximum. However, propagation of mesoscale convective elements is parallel to the ambient wind field in the Pacific Ocean whereas it is orthogonal to the ambient wind in the eastern Indian Ocean/Bay of Bengal region. In both locations, the elements appear to have propagation speeds similar to inertial-gravity modes and can persist for a number of days.
   - Overall, despite the differences in propagation characteristics, the observations suggest similarity between organized convection in JASMINE and TOGA COARE. This type of sloping midlevel inflow transporting momentum downward in the stratiform region was identified by Kingsmill and Houze (1999a) and Houze et al. (2000) from TOGA COARE ship and aircraft Doppler radar data. Houze et al. (2000) determined that this midlevel downward inflow acted as a positive feedback enhancing the low-level westerlies in the warm

pool intraseasonal oscillation. Thus, all the elements of a positive momentum feedback appear to have been present in the Bay of Bengal region.

Whereas JASMINE provided substantial insight into the coupled ocean–atmosphere structure in the eastern Indian Ocean region, there remain many unanswered questions that require further investigation. Some of these questions are highlighted below:

1) The intraseasonal variability observed during JASMINE indicates very strong ocean–atmosphere interactions in the Bay of Bengal and the eastern Indian Ocean. But what is the impact of intraseasonal wind forcing on the broaderscale Indian Ocean and its overall heat balance?
2) Detailed observations of an intraseasonal oscillation during its mature phase in the Bay of Bengal were made during JASMINE. But the oscillation appears to be a basinwide phenomena (e.g., Lawrence and Webster 2002) propagating along the equator before extending northward in the eastern part of the Indian Ocean and the Bay of Bengal. What are the processes that generate this basinwide phenomenon and determine its westward and northward speed of propagation?
3) There appears to be some similarity in the surface fluxes and the tropospheric moisture distribution between the undisturbed star-1 period and the TOGA COARE period 1. From a detailed numerical modeling study, Parsons et al. (2000) was able to suggest that subsiding dry continental air was responsible for the suppressed convection over the warm pool of the western Pacific. Are similar controls occurring during monsoon break periods and is the source of subsiding midtropospheric air at these times also of higher-latitude continental origin?
4) The JASMINE observations suggest a very strong interaction between the atmosphere and the ocean on these timescales, which is both dynamical and thermodynamical. Given that most atmosphere general circulation models have a near absence of intraseasonal oscillations in model simulations (e.g., Slingo et al. 1996) it is hoped that the JASMINE results will be used to define a modeling strategy for the simulation of intraseasonal oscillations. Given the degree of interaction between the ocean and the atmosphere, as was observed in JASMINE, it is likely that the modeling of intraseasonal variability may have to employ a coupled model strategy.

The dataset obtained during JASMINE is unique in the sense that it obtained time series of data in a location of the Tropics in which few observations had been made. Furthermore, JASMINE measured concurrently the structure of the ocean, the ocean–atmosphere interface, and the atmosphere including clouds and convection. It is anticipated that these data will be used to determine fundamental processes that control how the ocean and the atmosphere interact on intraseasonal timescales. The data collected will also allow the fundamental rationale of JASMINE to be addressed: the improvement of numerical simulations and predictions of monsoon phenomena. From an oceanic perspective, this goal is being approached by attempting to replicate the JASMINE ocean observations (e.g., HWHL). Furthermore, work is currently under way to compare single-column realizations of ECMWF model output with column observations from JASMINE. The aim of this comparison is to determine commonalities and differences between incolumnar heating in intensely convective regions. This procedure is based on the hypothesis that intraseasonal variability is absent from many numerical modes because convective available potential energy is released too quickly in numerical models and does not build up to the levels encountered in the undisturbed tropical atmosphere prior to the existence of an intraseasonal event (T. N. Palmer, ECMWF, 2000, personal communication).

Based upon what was found in the JASMINE Pilot Study and on the newly emerging ideas regarding phenomenology in the Indian Ocean–monsoon regime, several research plans are under consideration. One is to conduct a more expansive survey of the coupled ocean–atmosphere interaction on intraseasonal timescales in the central and eastern Indian Ocean during 2003–04. The aim would be to obtain detailed surface flux and evolving ocean and atmospheric structures for a longer period during the established summer monsoon. Major emphases might be on the determination of the wider field responses of the upper ocean to intraseasonal atmospheric forcing and the determination of the spatial and temporal patterns of interface fluxes. The timing of a JASMINE II would be crucial and tied to the maximum coverage of satellites during the 2002–05 period. The process study is planned to take place within the Global Energy and Water Cycle Experiment (GEWEX) Coordinated Enhanced Observing Period (CEOPS). Another plan is to develop an Indian Ocean monsoon observing system to study and monitor the Indian Ocean zonal mode or dipole (Webster et al. 1999; Saji et al. 1999; Yu and Rienecker 1999, 2000). Such an effort requires

the maintenance of the XBT lines already in the Indian Ocean, the deployment of the Argo (profiling temperature and salinity floats) array, and deployment of a tropical moored buoy array spanning the Indian Ocean. These two major plans are being considered in detail by the Asian–Australian Monsoon Panel of World Climate Research Programme's Climate Variability and Predictability Study (CLIVAR).

ACKNOWLEDGMENTS. The planning for JASMINE emerged out of the St. Michael's Conference on the Variability of the Asian–Australian monsoon system held in July 1998, funded by the Climate Dynamics and Large-Scale Dynamic Meteorology Programs of the Atmospheric Sciences Division (ATM) of the National Science Foundation (NSF), the National Oceanic and Atmospheric Administration (NOAA) Office of Global Programs (OGP), and NASA. Funding for the JASMINE Pilot Study came from NSF/ATM and NSF/OCE (Physical Oceanography Program), and NOAA/OGP. Specifically, support was provided through NSF Grants ATM-9900710, NSF-ATM-9820531, and NOAA/OGP Grant NA67RJ0154 for the University of Colorado and NOAA/ETL; ATM-9900710 and NOAA Cooperative Agreement NA67RJO155 for the University of Washington group; and by NSF ATM-9820531 and NOAA/OGPNA67RJ0154 for the Hawaii group. Financial support from NASA allowed the deployment of the cloud radar. The NOAA Environmental Technology Laboratories provided equipment and resources. Support for the Australian part of the field phase came from the Marine Sciences Division of CSIRO.

ECMWF made their data available for the period of the cruise for analysis. For this we appreciate the efforts of Drs. M. Miller and A. Hollingsworth. Prof. R. H. Johnson and Dr. P. E. Ciesielski kindly provided analyzed aerological data from TOGA COARE. Geostationary satellite data from the *METEOSAT-5* was made available by the European Space Agency through the efforts of Drs. R. Sadourny, J.-L. Monge, and M. Dubois. We would like to thank the crew of the NOAA ship *Ronald H. Brown* and the *Franklin.* We would also like to acknowledge the constructive comments of Prof. J. A. Curry.

APPENDIX: JASMINE: OBSERVING INTRASEASONAL OSCILLATIONS OF THE MONSOON.

JASMINE was a bilateral effort of the United States and Australia under the auspices of CLIVAR. Four U.S. research groups and an Australian group collaborated in the planning and execution of JASMINE, each with specific responsibilities. The University of Colorado [Principal Investigator (PI): P. J. Webster] and the NOAA Environmental Technology Laboratory (NOAA/ETL PI: C. W. Fairall) were responsible for the measurement of the air–sea fluxes. The University of Hawaii group (PIs: P. Hacker, R. Lukas, and E. Firing) was responsible for the measurement and analysis of the upper-ocean temperature, salinity, and velocity fields during the monsoon onset period. The University of Washington group (PIs: R. Houze Jr., S. Yuter, and Y. Serra) documented the evolution of convection and its relationship to monsoon transitions. Both the University of Colorado/NOAA-ETL and the University of Washington groups maintained an upper-air sounding program throughout JASMINE. These four principal research groups used the *Brown* as their principal observing platform. The fifth research group participating in JASMINE was from the Australian CSIRO Marine Sciences Division (PIs: J. S. Godfrey and E. F. Bradley) that used the *Franklin.* They were responsible for measuring upper-ocean heat, salt, and momentum budgets; air–sea fluxes; and atmospheric structure during the late summer monsoon. E. F. Bradley also represented the Australian group aboard the *Brown.*

REFERENCES

Bhat, G. S., and Coauthors, 2001: BOBMEX—The Bay of Bengal Monsoon Experiment. *Bull. Amer. Meteor. Soc.,* **82,** 2217–2243.

Chang, H.-R., and R. L. Grossman, 1999: Evaluation of the bulk surface algorithms for light wind conditions using data from the Coupled Ocean–Atmosphere Response Experiment (COARE). *Quart. J. Roy. Meteor. Soc.,* **125,** 1551–1588.

Charney, J. G., and J. Shukla, 1981: Predictability of monsoons. *Monsoon Dynamics,* J. Lighthill, Ed., Cambridge University Press, 99–110.

Chen, S. S., R. A. Houze, and B. E. Mapes, 1996: Multiscale variability of deep convection in relation to large-scale circulation in TOGA COARE. *J. Atmos. Sci.,* **53,** 1380–1409.

Donlon, C. J., and Coauthors, 1998: Solid-state radiometer measurements of sea surface skin temperature. *J. Atmos. Oceanic Technol.,* **15,** 775–787.

Ecklund, W. L., D. A. Carter, and B. B. Balsley, 1988: A UHF profiler for the boundary layer: Brief description and initial results. *J. Atmos. Oceanic Technol.,* **5,** 432–441.

——, C. R. Williams, P. E. Johnston, and K. S. Gage, 1997: A 3-GHz profiler for precipitating cloud studies. *J. Atmos. Oceanic Technol.,* **16,** 309–322.

Edson, J. B., A. A. Hinton, K. E. Prada, J. E. Hare, and C. W. Fairall, 1998: Direct covariance flux estimates from moving platforms at sea. *J. Atmos. Oceanic Technol.,* **15,** 547–562.

Fairall, C. W., E. F. Bradley, D. P. Rogers, J. B. Edson, and G. S. Young, 1996: Bulk parameterization of air–sea fluxes for the Tropical Ocean–Global Atmosphere Coupled–Ocean Atmosphere Response Experiment. *J. Geophys. Res.,* **101,** 3747–3764.

——, A. B. White, J. B. Edson, and J. E. Hare, 1997: Integrated shipboard measurements of the marine boundary layer. *J. Atmos. Oceanic Technol.,* **14,** 338–359.

——, P. O. G. Persson, E. F. Bradley, R. E. Payne and S. P. Anderson, 1998: A new look at calibration and use of Eppley precision infrared radiometers: Part 1, Theory and application. *J. Atmos. Oceanic. Technol.,* **15,** 1230–1243.

——, J. E. Hare, J. B. Edson, and W. McGillis, 2000: Parameterization and micrometeorological measurement of air–sea gas transfer. *Bound.-Layer Meteor.,* **96,** 63–105.

Feng, M., R. Lukas, P. Hacker, R. A. Weller, and S. P. Anderson, 2000: Upper-ocean heat and salt balances in the western equatorial Pacific in response to the intraseasonal oscillation during TOGA COARE. *J. Climate,* **13,** 2409–2427.

Ferranti, L., J. M. Slingo, T. N. Palmer, and B. J. Hoskins, 1997: Relations between interannual and intraseasonal monsoon variability as diagnosed from AMIP integrations. *Quart. J. Roy. Meteor. Soc.,* **123,** 1323–1357.

Frisch, A. S., C. W. Fairall, and J. B. Snider, 1995: On the measurement of stratus cloud and drizzle parameters with a K-band Doppler radar and a microwave radiometer. *J. Atmos. Sci.,* **52,** 2788–2799.

Gadgil, S., and S. Sanjani, 1998: Monsoon precipitation in the AMIP runs. *Climate Dyn.,* **14,** 659–689.

Gage, K. S., C. R. Williams, and W. L. Ecklund, 1996: Application of the 915-MHz profiler for diagnosing and classifying tropical precipitating cloud systems. *Meteor. Atmos. Phys.,* **59,** 141–151.

——, ——, ——, and P. E. Johnston, 1999: Use of two profilers during MCTEX for unambiguous identification of Bragg scattering and Rayleigh scattering. *J. Atmos. Sci.,* **56,** 257–270.

Godfrey, J. S., 1995: The role of the Indian Ocean in the global climate system: Recommendations regarding the global ocean observing system. Report of the Ocean Observing System Development Panel, Background Rep. 6, Texas A&M University, College Station, TX, 89 pp.

——, R. A. Houze, R. H. Johnson, R. Lukas, J. L. Redelsperger, A. Sumi, and R. Weller 1998: Coupled Ocean–Atmosphere Response Experiment (COARE): An interim report. *J. Geophys. Res.,* **103C,** 14 395–14 450.

——, E. F. Bradley, P. A. Coppin, L. F. Pender, T. J. McDougall, E. W. Schulz, and I. Helmond, 1999: Measurement of upper ocean heat and freshwater budgets near a drifting buoy in the equatorial Indian Ocean. *J. Geophys. Res.,* **104,** 13 269–13 302.

Hacker, P., E. Firing, J. Hummon, A. L. Gordon, and L. Kindle, 1998: Bay of Bengal currents during the northeast monsoon. *Geophys. Res. Lett.,* **25,** 2769–2772.

Han, W., D. Lawrence, and P. J. Webster, 2001: Dynamical response of equatorial Indian Ocean to intraseasonal winds: Zonal flow. *Geophys. Res. Lett.,* **28,** 4215–4218.

Hogg, D. C., F. O. Guiraud, J. B. Snider, M. T. Decker, and E. R. Westwater, 1983: A steerable dual-channel microwave radiometer for measurement of water vapor and liquid in the atmosphere. *J. Climate Appl. Meteor.,* **22,** 789–806.

Houze, R. A., Jr., S. S. Chen, D. E. Knigsmill, Y. Serra, and S. E. Yuter, 2000: Convection over the Pacific warm pool in relation to the atmosphere Kelvin–Rossby wave. *J. Atmos. Sci.,* **57,** 3058–3089.

Johnson, R. H., and P. E. Ciesielski, 2000: Rainfall and radiative heating rates from TOGA COARE atmospheric budgets. *J. Atmos. Sci.,* **57,** 1497–1514.

Kingsmill, D. E., and R. A. Houze, 1999a: Kinematic characteristics of air flowing into and out of precipitating convection over the west Pacific warm pool: An airborne Doppler radar survey. *Quart. J. Roy. Meteor. Soc.,* **125,** 1165–1207.

——, and ——, 1999b: Thermodynamic characteristics of air flowing into and out of precipitating convection over the west Pacific warm pool. *Quart. J. Roy. Meteor. Soc.,* **125,** 1209–1229.

KWAJEX, cited 1999: TRMM Kwajalein Experiment**.** [Available online at http://www.atmos.washington.edu/kwajex/.]

Lawrence, D. M., and P. J. Webster, 2001: Interannual variations of the intraseasonal oscillation in the south Asian summer monsoon region. *J. Climate,* **14,** 2910–2922.

——, and ——, 2002: The boreal summer intraseasonal oscillation: Relationship between northward and eastward movement of convection. *J. Atmos. Sci.,* **59,** 1593–1606.

Loschnigg, J., and P. J. Webster, 2000: A coupled ocean–atmosphere system of SST modulation for the Indian Ocean, *J. Climate,* **13,** 3342–3360.

Lukas, R., and E. Lindstrom, 1991: The mixed layer of the western equatorial Pacific Ocean. *J. Geophys. Res.,* **96,** 3343–3357.

——, P. Hacker, S. DeCarlo, J. Hummon, F. Santiago-Mandujano, and D. Wright, 2001: Hydrographic Observations during the Joint Air–Sea Monsoon

Interaction Experiment (JASMINE) Pilot Study: Data Report. School of Ocean and Earth Science and Technology (SOEST) Rep. 5319, University of Hawaii at Manoa, 246 pp. [Available online at http://www.soest.hawaii.edu/JASMINE/.]

Masson, S., P. Delecluse, J.-P. Boulenger, and C. Menkes, 2002: A model study of the seasonal variability and formation mechanisms of the barrier layer in the eastern Indian Ocean. *J. Geophys. Res.,* **107C,** in press.

McCreary, J. P., P. K. Kundu, and R. L. Molinari, 1993: A numerical investigation of the dynamics, thermodynamics and mixed-layer processes in the Indian Ocean, *Prog. Oceanogr.,* **31,** 181–244.

Meehl, G. A., 1994: Coupled ocean–atmosphere–land processes and south Asian monsoon variability. *Science,* **265,** 263–267.

Murty, V. S. N., Y. V. B. Sarma, D. P. Rao, and C. S. Murty, 1992: Water characteristics, mixing and circulation in the Bay of Bengal during the southwest monsoon. *J. Mar. Res.,* **50,** 207–228.

Oberhuber, J. M., 1988: An atlas based on the COADS data set: The budgets of heat, buoyancy and turbulent kinetic energy at the surface of the global ocean. Max-Planck-Institut für Meteorology Rep. 15, 20 pp., and 160 figs.

Palmer, T. N., 1994: Chaos and the predictability in forecasting the monsoons. *Proc. Indian Natl. Sci. Acad.,* **60A,** 57–66.

Parsons, D. B., K. Gryanik, C.-H. Moeng, D. J. Olbers, and T. H. Warncke, 2000; The evolution of the tropical western Pacific atmosphere–ocean system following the arrival of a dry intrusion. *Quart. J. Roy. Meteor. Soc.,* **126,** 517–548.

Ramanathan, V., and Coauthors, 2001: The Indian Ocean Experiment: An Integrated Assessment of the Climate Forcing and Effects of the Great Indo-Asian Haze. *J. Geophys. Res.,* **106** (D22), 28 371–28 399.

Saji, N. N., B. N. Goswami, P. N. Vinayachandran, and T. Yamagata, 1999: A dipole mode in the tropical Indian Ocean. *Nature,* **401,** 360–363.

Schott, F., 1976: Response of the Indian Ocean to change of monsoon and the Indian-Ocean Experiment. *Meteor. Rundschau,* **29** (5), 133–141.

——, and J. P. McCreary Jr., 2001: The monsoon circulation of the Indian Ocean. *Progress in Oceanography,* Vol. 51, Pergamon, 1–123.

Sengupta, D., and M. Ravichandran, 2001: Oscillations of Bay of Bengal sea surface temperature during the 1998 summer monsoon. *Geophys. Res. Lett.,* **28,** 2033–2036.

——, B. N. Goswami, and R. Senan, 2001: Coherent intraseasonal oscillations of ocean and atmosphere during the Asian summer monsoon. *Geophys. Res. Lett.,* **28,** 4127–4130.

Sikka, D., and S. Gadgil, 1980: On the maximum cloud zone and the ITCZ over Indian longitudes during the southwest monsoon. *Mon. Wea. Rev.,* **108,** 1840–1853.

Slingo, J. M., and Coauthors, 1996: Intraseasonal oscillations in 15 atmospheric general circulation models: Results from an AMIP diagnostic subproject. *Climate Dyn.,* **12,** 325–357.

Snider, J. B., and D. A. Hazen, 1998: Surface-based radiometric observations of water vapor and cloud liquid in the temperate zone and in the Tropics. *Radio Sci.,* **33,** 421–432.

Sperber, K. R., and T. N. Palmer, 1996: Interannual tropical rainfall variability in general circulation model simulations associated with the Atmospheric Model Intercomparison Project. *J. Climate,* **9,** 2727–2750.

Swallow, J. C., 1980: The Indian Ocean Experiment. *Science,* **209,** 588–594.

Vialard, J., and P. Delecluse, 1998: An OGCM study for the TOGA decade. Part II: Barrier layer formation and variability. *J. Phys. Oceanogr.,* **28,** 1089–1106.

Webster, P. J., 1994: The role of hydrological processes in ocean–atmosphere interaction. *Rev. Geophys.,* **32,** 427–476.

——, and S. Yang, 1992: Monsoon and ENSO: Selectively interactive systems. *Quart. J. Roy. Meteor. Soc.,* **118,** 877–926.

——, and R. A. Tomas, 1999: An atlas of precipitation and boundary layer winds during intraseasonal oscillation events in the Indian Ocean 1985–1995 extended summer season. Program in Atmospheric and Oceanic Sciences Tech. Report, University of Colorado, Boulder, CO, 136 pp.

——, C. Clayson, and J. A. Curry, 1996: Clouds, radiation and the diurnal cycle of sea surface temperature in the tropical western Pacific Ocean. *J. Climate,* **9,** 1712–1730.

——, T. Palmer, M. Yanai, R. Tomas, V. Magana, J. Shukla, and A. Yasunari, 1998: Monsoons: Processes, predictability and the prospects for prediction. *J. Geophys. Res.,* **103** (C7), 14 451–14 510.

——, A. Moore, J. Loschnigg, and M. Leban, 1999: Coupled ocean–atmosphere dynamics in the Indian Ocean during 1997–98. *Nature,* **40,** 356–360.

——, C. Clark, G. Cherikova, J. Fasullo, W. Han, J. Loschnigg, and K. Sahami, 2001: The monsoon as a self-regulating coupled ocean–atmosphere system. *Meteorology at the Millennium,* R. Pearce, Ed., Academic Press, 198–219.

Weller, R. A., and S. P. Anderson, 1996: Surface meteorology and air–sea fluxes in the western equatorial Pacific warm pool during the TOGA Coupled

Ocean–Atmosphere Response Experiment. *J. Climate,* **9,** 1959–1990.
——, M. F. Baumgartner, S. A. Josey, A. S. Fisher, and J. C. Kindle, 1999: Atmospheric forcing in the Arabian Sea during 1994–1995: Observations and comparisons with climatology and models. *Deep-Sea Res. II,* **45,** 1961–1999.
Wyrtki, K., 1971: *Oceanographic Atlas of the International Indian Ocean Expedition.* National Science Foundation, 531 pp.
——, 1973: An equatorial jet in the Indian Ocean. *Science,* **181,** 262–264.
Yang, G. Y., and J. Slingo, 2001: The diurnal cycle in the Tropics. *Mon. Wea. Rev.,* **129,** 784–801.
Yu, L., and M. Rienecker, 1999: Mechanisms for the Indian Ocean warming during the 1997–98 El Niño. *Geophys. Res. Lett.,* **26,** 735–738.
——, and M. M. Rienecker, 2000: Indian Ocean warming of 1997–1998. *J. Geophys. Res.,* **105C,** 16 923–16 939.
Zuidema, P., 2003: Convective clouds over the Bay of Bengal. *Mon. Wea. Rev.,* in press.